Application of the Thermal Flash Technique for Characterizing High Thermal Diffusivity Micro and Nanostructures

By

LAURENT J MAJERUS

Submitted in partial fulfillment of the requirements
For the degree of Master of Science

Thesis Advisor: Dr. Alexis Abramson

Department of Mechanical and Aerospace Engineering
CASE WESTERN RESERVE UNIVERSITY

January, 2010

CASE WESTERN RESERVE UNIVERSITY

SCHOOL OF GRADUATE STUDIES

We hereby approve the thesis/dissertation of

Laurent J. Majerus

candidate for the Master of Science degree *.

(signed) Alexis R. Abramson

(chair of the committee)

Yasuhiro Kamotani

Joseph M. Prahl

(date) 10/22/09

*We also certify that written approval has been obtained for any proprietary material contained therein.

Table of Contents

List of Figures

List of Tables

Acknowledgements

Abstract

Chapter 1: Introduction

1.1 Introduction to Heat Transfer

1.2 Heat Conduction in Nanomaterials

1.3 Heat Conduction in Carbon Based Materials

1.3.1 Thermal Conductivity of Carbon Fibers

Chapter 2: Materials

2.1 Melt Spinning

2.1 Vapor Growth

2.1 Electrospinning of Polyimide

2.2 Fiber Preparation

Chapter 3: Experimental Methods

3.1 Previous Micro/Nano Thermal Characterization Techniques

3.1.1 Steady-State Techniques

3.1.2 Transient Techniques

3.2 Analytical Solutions

3.3 Data Analysis

3.4 Sensor Design

3.5 Heater Design

3.6 Experimental Approach

3.7 Thermal Flash Limitations

Chapter 4: Results and Discussion

4.1 Mitsubishi K13D2U

4.2 ASI Vapor Grown Carbon Fibers

4.3 University of Akron Composite Polyimide/Coal Tar Pitch Fibers

4.4 Conclusions

4.5 Future Work

Appendix

References

List of Figures

Figure 1: Moore's Law

Figure 2: 1D mass spring system

Figure 3: Dispersion Curve

Figure 4: Scattering Processes

Figure 5: Thermal Conductivity of Carbon Fibers

Figure 6: Melt Spinning Apparatus

Figure 7: 2D Representation of Pyrograf I Mats

Figure 8: Electrospinning Process

Figure 9: Collector for Spinning of Composite Fibers

Figure 10: Heat Flow Meter

Figure 11: Method from Kim et al.[20]

Figure 12: T-type Sensor

Figure 13: 3-omega Method

Figure 14: OHETS and TPET method

Figure 15: TET method

Figure 16: 1D Model for Analytical Solution

Figure 17: 3D Model of Full SEM Stage

Figure 18: Heater Temperature vs. Current

Figure 19: SEM image of Mitsubishi Fiber Testing

Figure 20: Delta Mode Technique

Figure 21: SEM Image of a Mitsubishi Fiber on an Aluminum Sensor

Figure 22: Fit Between Analytical Solution and Experimental Data for a Mitsubishi Fiber

Figure 23: Summary of Measured Thermal Diffusivities for Mitsubishi Carbon Fiber

Figure 24: Fit Between Experimental Data and Analytical Solution for a Short ASI Pyrograf I Fiber

Figure 25: SEM Image of Pyrograf I Bundle Testing

Figure 26: Summary of Pyrograf I Measurements

Figure 27: Apparatus for Placing Composite Fibers

Figure 28: SEM Image of Composite Fibers on Aluminum Sensor

Figure 29: Graph of Composite Fibers Thermal Conductivity vs. Pitch Percentage

Figure 30: Optical Images of Composite Fibers Depicting Unabsorbed Pitch

Figure 31: Updated Graph of Composite Fibers Thermal Conductivity vs. Pitch Percentage with New Fit

Figure 32: Micro-scale Mechanical Strain Device

Figure 33: 1D Model for Analytical Solution

Figure 34: Cauchy's Theorem

Figure 35: Mitsubishi Measurements with Error

Figure 36: ASI Measurements with Error

List of Tables

Table 1: Summary of all Measurements

Table 2: Measurements Including Standard Error

Acknowledgements

I would like to thank the following individuals for the role they played in helping to prepare this work:

Dr. Alexis Abramson for providing me with this project and guiding me toward its completion

Professor Cakmak and student Han Yan from the University of Akron for preparing polyimide/pitch samples

Max Lake, David Burton, and Andrew Palmer from Applied Sciences Inc. for providing Pyrograf I samples

Fellow nanoEngineering labmates for many suggestions and help along the way

My friends and family for all their loving support

Application of the Thermal Flash Technique for Characterizing High Thermal Diffusivity Micro and Nanostructures

Abstract

By

LAURENT J MAJERUS

Developments in modern electronics are hindered by smaller devices creating more heat without better cooling methods. Better heat dissipating materials are sought to lower operating temperatures, and an increasing number of micro and nanostructures are being developed for such use. Testing these one dimensional structures is difficult due to their microscopic scale, so a new method is developed for measuring the thermal properties of high thermal diffusivity micro and nanofibers. This method builds upon previous techniques to remove inaccuracies and unnecessary complications. The result is the thermal flash technique used here to measure the thermal properties of a variety of carbon based structures, focusing on a fiber composed of polyimide and coal tar pitch developed at the University of Akron. An investigation into the thermal properties of these fibers as a function of pitch is presented, and the results compare within +/- 5% to reported values in the literature.

Chapter 1: Introduction

Over the past several decades advances in electronics have come about mainly due to the miniaturization or scaling of these devices into the nanoscale regime. This miniaturization has led to faster, denser, and more efficient electronics with wide ranging application. The field of nanoscience, or the study and control of matter on an atomic scale, can help bring about greater performance through the development of unique nanoscaled structures. Unfortunately, nanoscale research has mainly focused on studying and improving the electrical, mechanical, and photonic properties of materials, and an attempt to improve the thermal performance of materials has received very little attention, thus conventional heat dissipating materials such as copper and aluminum are no longer good enough. Thermal management is becoming an increasingly serious problem that is limiting the development of even faster, smaller, denser packed electronics. The key to addressing this concern for better heat generating materials is to understand how heat is transported at the nanoscale and then developing materials that exploit these phenomenon.

Computer chip power densities are increasing at an alarming rate as shown in Figure 1. Unfortunately the same materials used to cool first generation chips, such as copper and aluminum, are still being used today, even with the availability of carbon fibers with thermal conductivities four times higher![1] Today's chips must thus operate at higher temperatures than those from a decade or more ago, resulting in decreased lifetimes and reduced reliability. In order to progress to smaller and faster computer chips, new materials for thermal management must be found.

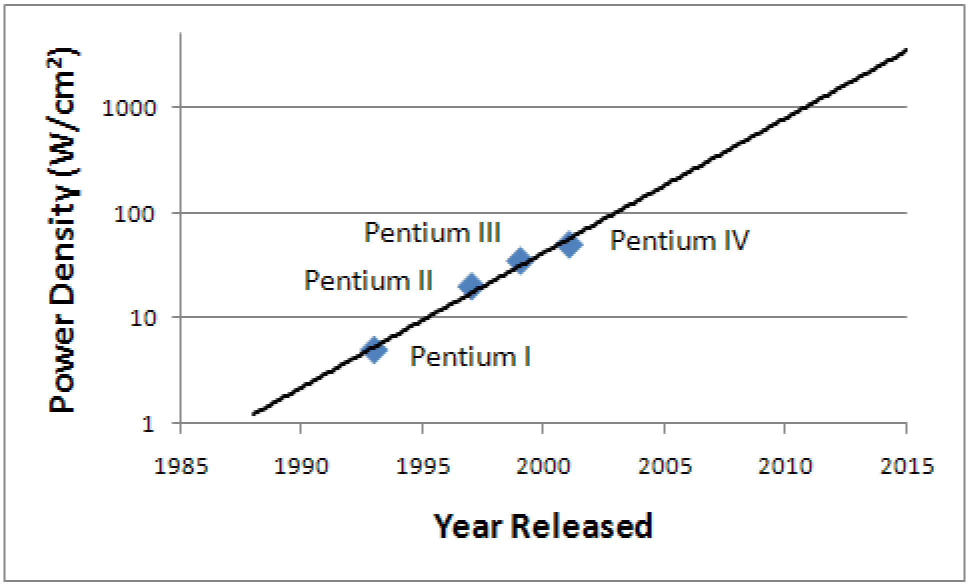

Figure 1: According to Moore's Law, the number of transistors on a computer chip doubles every two years, which also accounts for a doubling of power consumption every 18 months. All this power consumed by the chip leads to an ever increasing heat dissipation problem.[2]

When examining the literature for heat dissipation solutions, it is clear that graphite structured materials are the leading candidates for next generation thermal management materials. The unique structure of graphite allows many carbon materials to exhibit very high thermal conductivities, especially micro and nanoscaled fibers and tubes.[3] However, using such small materials to fabricate bulk thermal conductors is very complicated. By studying the properties of individual fibers, the performance of thermal composites may be predicted and could lead to the development of better materials. Here, a new technique has been developed, improved and employed for use in testing several high thermal diffusivity fibers. It is a transient technique thus being quick and not requiring steady-state conditions. For the technique, a fiber is suspended between a sensor and an insulating prop prior to testing. The sensor is an aluminum wire over which a current is pulsed. During the pulses the voltage is measured and recorded. A heater is then brought into contact with the fiber and heat flows into the sensor due to thermal conduction. As the temperature of the sensor increases, its resistance will change, as resistance is a function of temperature. This resistance change will cause an exponential voltage change which is recorded and used to calculate the thermal diffusivity of the fiber being tested.

Chapter 1 provides the reader with a brief review of thermal conduction, explains why carbon based materials are the focus of this work, and finally summarizes the literature studies of thermal conductivity of carbon fibers. Chapter 2 introduces the materials studied in this work. The measurement technique was first validated using Mitsubishi K13D2U melt spun carbon fibers, due to availability and size. Next, an extremely conductive vapor-grown fiber was tested, Pyrograf I from Applied Sciences Inc. This fiber has an extremely high thermal conductivity that posed as an interesting measurement challenge as well as further validation of the technique's accuracy. Finally a series of newly developed fibers produced at the University of Akron by Han Yan and Professor Cakmak were studied. These fibers were produced through electrospinning and were produced for use in next generation thermal management materials. Chapter 3 presents the transient thermal flash method developed to reduce and eliminate problems of previous techniques. Finally, Chapter 4 is a summary of all measurements performed and discusses the importance of the results.

1.1 *Introduction to Heat Transfer*

Heat transfer is thermal energy in transit due to a temperature difference.[4] Whenever a temperature difference exists between two surfaces or media, heat transfer will occur until a thermal equilibrium is established. Due to the second law of thermodynamics, heat transfer must always occur from a relatively hot medium to a colder one. There are three modes of heat transfer including conduction, convection, and thermal radiation. Conduction refers to heat transfer that occurs within either a solid or a stationary fluid. Convection is a mode of heat transfer occurring due to the relative movement of a fluid over another surface. Lastly, thermal radiation is a heat transfer mode caused by electromagnetic waves. Every surface emits electromagnetic waves with energy proportional to their temperature, and these waves will cause heat transfer if a temperature gradient exists between two or more surfaces. The following section will focus on conduction heat transfer as it is the prevalent heat transfer mode for this work.

Conduction occurs due to atomic interactions within a solid medium. Heat is transported in a solid by atomic lattice vibrations and by the motion of free electrons and holes. In metals, free electrons are the dominant mode of heat transfer, by moving heat along a temperature gradient. For highly doped semiconductors, holes can provide a significant form of heat transfer; but typically lattice vibrations are the dominant mode of heat transfer in non-metals. In order to characterize how well a material conducts heat a quantity known as thermal conductivity (k) must be defined. Thermal conductivity as defined by Fourier's Law is a measure of how much heat (q) a material conducts as it is applied to a thermal gradient (∇T):

$$q = -k \nabla T \tag{1.1}$$

The higher a material's thermal conductivity, the greater the amount of heat it will conduct when it encounters a thermal gradient. Another measure of a material's ability to transport heat is thermal diffusivity (α) which describes how fast heat moves through a medium. Thermal diffusivity can be related to thermal conductivity by,

$$\alpha = \frac{k}{\rho\, C_p} \tag{1.2}$$

with ρ being the density of the material and C_p being its specific heat capacity. This work deals with non-metallic materials, therefore the focus will be on atomic lattice vibrations.

In order to study atomic lattice vibrations it is useful to picture the atoms in a lattice connected by springs rather than chemical bonds. This is not a bad model because in actuality atoms are not rigidly fixed to one another and can move much like a mass-spring system. Looking at the simplest case first, we can imagine a line of atoms equally spaced with springs connecting them as in Figure 2. By displacing the atom at position S, the surrounding atoms must move to balance out the energy, and this displacement can move through a lattice as a wave. These lattice vibrations are more formally known as phonons and are analogous to photons in their representation as wave packets with the properties of particles.

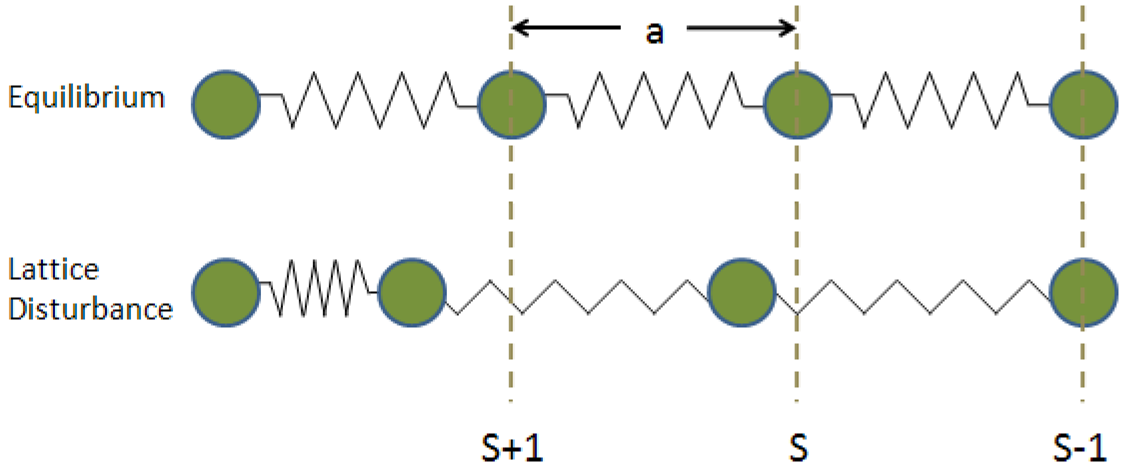

Figure 2: This cartoon represents atomic vibrations with a one dimensional mass spring system. The bottom line demonstrates what happens when the ball at S is disturbed from its equilibrium position.

Atomic displacements along the line can either be up and down or left and right. By moving an atom left or right, longitudinal waves are formed because the direction of atomic displacement is in the same direction as wave propagation, while atomic motion up and down creates transverse waves. In order to determine the angular frequency of phonon waves we must set up and solve the equations of motion. The first step is to set up a force balance on one of the atoms in then line, say the atom at point S, to give the set of difference equations:

$$-m\frac{d^2u_s}{dt^2} = C(u_{s+1} + u_{s-1} - 2u_s) \qquad (1.3)$$

In this equation u is the displacement of the atoms, m is the mass of the atom, C is the spring constant, and s is merely an index to identify individual atoms. We must then guess a solution that will solve our equation of motion. Because we know that phonons move as waves, our guess is of the form:

$$u_s = u_0 e^{i(Kna - \omega t)} \tag{1.4}$$

In this equation K is the phonon's wavenumber, where K = 2π/λ, and a is the atomic spacing of the atoms at equilibrium. By plugging this solution into our force balance, we can solve for the angular frequency:

$$\omega^2 = \frac{2C}{m}(1 - \cos Ka) \tag{1.5}$$

Now that we know the angular frequency of our phonons we can characterize several important concepts. The Brillouin zone is defined as the primitive zone of a reciprocal lattice. Only the frequencies within the first Brillouin zone, where:

$$K = \pm\frac{\pi}{a} \tag{1.6}$$

are actually independent. Any other values of K are merely a reflection of lattice motion within the first Brillouin zone.

The dispersion relation is defined as the correlation between ω and K, and is often plotted similarly to Figure 3. An important quantity which may be found from the dispersion relation is the group velocity, or the speed of the phonon waves. The group velocity can be calculated by taking the slope of the dispersion curve, defined as:

$$v_g = \frac{d\omega}{dK} \tag{1.7}$$

For the one-dimensional crystal with the mass spring system, the group velocity would be:[5]

$$v_g = \sqrt{\frac{C}{2m}} \cdot \frac{a \sin Ka}{\sqrt{1 - \cos Ka}} \tag{1.8}$$

In crystals with only one atom per primitive cell such as the one we have constructed, there exist only acoustical branches in the dispersion relation. When a primitive cell contains two or more atoms, optical branches begin to exist. The optical branch is the higher curve in Figure 3, and has a lower slope than the acoustical branch. Because the acoustical branch has a higher slope, it has a higher group velocity, thus contributing more to the thermal conductivity of the material than the optical branches.

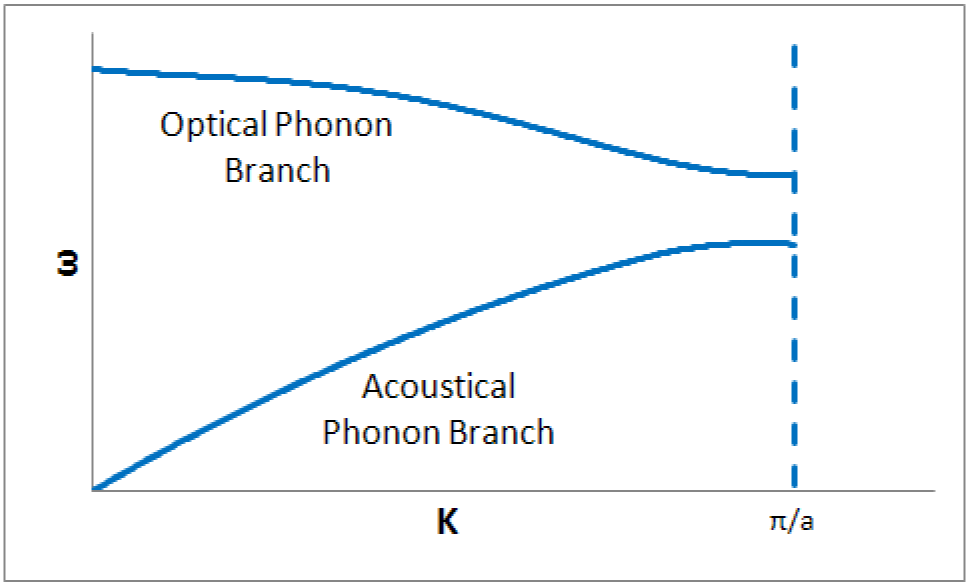

Figure 3: Example of a dispersion curve showing both acoustic and optical paths. The slope of the curve is the group velocity.

In order to discuss how phonon transport can deviate from expected and theoretical predictions the term mean free path must be defined. The mean free path of a phonon is the average distance it travels before colliding with or scattering off a defect, another phonon, boundary, etc. The mean free path is defined as:

$$l = v\tau \tag{1.9}$$

where v is the velocity of the phonon and τ is the average time between collisions or scattering. It is often very difficult to calculate a value for τ, and thus a good estimate of the mean free path of a material can be found using kinetic theory:[5]

$$l = \frac{3k}{Cv} \tag{1.10}$$

Here k is the material's thermal conductivity and C is the heat capacity per unit volume. It should be realized that this is only an estimate of the mean free path and is not always accurate for many reasons, mostly due to phonon's dispersive nature causing group velocities to vary depending on the frequency.

To make sense of the concept of a phonon's mean free path, it is best to examine some of the inelastic scattering mechanisms. Although we conceptualize phonon motion by balls and springs, in truth the forces between atoms are not purely harmonic, and the spring constant is a function of the atom's displacement. Phonon waves are not said to have any momentum, however, they do still interact with one another as if they do have momentum. There are two types of phonon-phonon scattering processes, normal and umklapp processes, which are depicted in Figure 4. Normal scattering is what you would expect from classical physics and conservation of momentum, such as two waves with different wave vectors combining to create a wave with a third wave vector, for example:

$$\overrightarrow{K_1} + \overrightarrow{K_2} = \vec{K}_3 \tag{1.11}$$

The reverse of this process may occur as well, with one phonon wave splitting to form two different waves. In these normal scattering mechanisms momentum is conserved, thus not having a serious impact on thermal conduction.

The second scattering process, umklapp, is important for determining a material's thermal conductivity, because now momentum is no longer conserved. This process is a bit more complicated than normal scattering, but occurs similarly to the normal process described above. Two waves form together to try to create a single phonon, however, due to the discrete nature of the atomic lattice, if the wavevector of the combined wave is outside of the Brillouin zone, then this process can only occur by the addition of the reciprocal lattice vector G:

$$\overrightarrow{K_1} + \overrightarrow{K_2} = \vec{K}_3 + \vec{G} \tag{1.12}$$

The addition of the reciprocal lattice vector G only serves to relate a wavenumber outside of the Brillouin zone to an equivalent one inside of the zone. Essentially this addition will drop the phonon into a lower frequency and wavevector, but also reverse the phonon's direction contributing to the randomness of thermal diffusion. Contrary to the normal scattering effects, umklapp processes do not conserve momentum and thus reduce heat flow through a material.

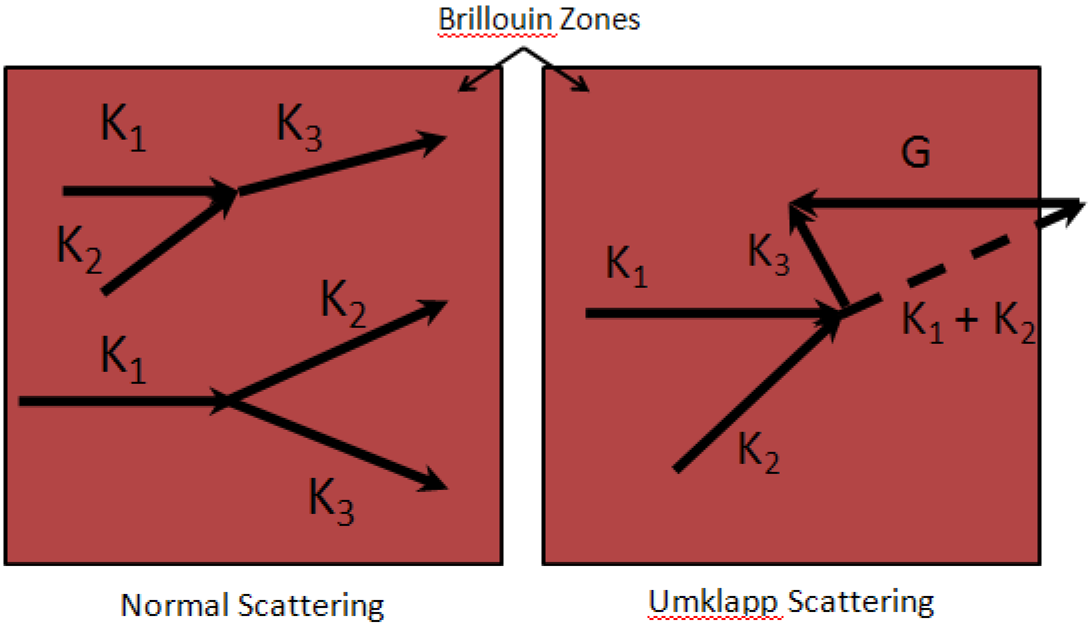

Figure 4: In normal scattering, two wavevectors collide to create a third wavevector that falls within the Brillouin zone or one wavevector splits to form two wavevectors that fall within the Brillouin zone. In umklapp scattering when two wavevectors collide the formed wavevector falls outside of the Brillouin zone so a reciprocal lattice vector is needed to create an equivalent wavevector within the zone.

Umklapp processes are not the only scattering mechanisms that will reduce the thermal conductance of a material. Other scattering effects such as those due to defects, impurities, dislocations, and boundaries also exist. The mean free path of a phonon in a material is thus a combination of the phonon-phonon scattering due to umklapp processes as well as scattering caused by boundaries, defects, dislocations, and impurities.

In summary, thermal conduction is the dominant focus of this work, and in the carbonaceous materials studied, phonons are the primary mechanism for heat transfer. Thermal conduction is directly related to the speed of phonons in a material, or the group velocity. However, material defects as well as umklapp scattering serve to decrease wave speed and hinder thermal conduction. All the processes mentioned above were developed for studying bulk materials, but when dealing with nanoscaled samples heat conduction can change.

1.2 Heat Conduction in Nanomaterials

By reducing the size of a material, the surface area becomes an increasingly larger percentage of the overall material. In the above description of phonon transport it was always assumed that the atoms were far inside the boundary of a material, and the lines of atoms continued infinitely in both directions. For a large bulk sample this is a valid assumption, but this no longer holds for nanomaterials. The surfaces are now extremely large compared to the overall volume of the material and the edges cannot be neglected. Other effects such as phonon confinement and quanitization can cause decreases in the phonon group velocities.

The increased surface area-to-volume ratio adds additional boundary and interface scattering mechanisms that do not play a significant role in bulk materials. All these interactions tend to decrease a material's thermal conductivity as the size of the material is reduced. When phonons encounters surface defects they normally interfere like waves, because the phonon's wavelength is much greater than the surface roughness. However, when the wavelength of the phonon becomes smaller or equal to the average surface roughness, phonons scatter diffusely as particles. This increased scattering will serve to decrease the thermal conductivity of a material.

Not all nanomaterials exhibit decreased thermal conductivities. Carbon nanotubes (CNTs), for example, exhibit extremely high thermal conductivities due their unique nanoscale structure. CNTs are comprised of rolls of graphene planes, and for single walled carbon nanotubes all the atoms located on the surface of the material. Phonons all move axially in the carbon nanotube because of its seamless structure. With all the phonons moving on the surface there is no place for them to scatter if the tube is defect free. The distinctive structure of carbon nanotubes allows extremely high phonon velocities with very little scattering leading to a very high thermal conductivity.[6]

1.3 Introduction to Carbon Based Materials

For nonmetals such as carbon based materials, phonons are the dominant heat carrier. Because phonon transport is closely related to the strength of the bonds in a material, diamond has historically been considered the best thermal conducting material. Diamond has stiff sp^3 bonds which allow its phonons to have very high velocities. However, the bonds that make up single carbon sheets, known as graphene, are sp^2 bonds that have been shown to be 33% stronger than diamonds sp^3 bonds.[6] Based on this fact, the phonon velocities in graphene are even higher than in diamond. The reason other carbon materials such as graphite do not exhibit higher thermal conductivity than diamond is because graphite is composed of many sheets of graphene with weak Van der Waals forces holding together the various layers. These weak bonds between the many layers in graphite cause a lot of phonon scattering and decrease its overall thermal conductance. Graphene sheets are difficult to isolate, and using graphene to build a useful heat conducting material is not feasible today. However, modern graphite based micro and nanomaterials, such as carbon fibers, have been known since the 1980s to have thermal conductivities much higher than copper and aluminum.[1,7,8]

Carbon nanotubes are today's ultimate thermal conductors, and have been found to be comprised of sheets of graphene rolled into tubes. Carbon nanotubes are thus composed of the very stiff sp^2 bond and due to its seamless tubular structure, the mean free path in carbon nanotubes is very long.[9] Due to the interesting structure of carbon nanotubes, they are thought to have the highest known thermal conductivity of today's materials. A recent molecular dynamics simulation by Berber et al. found that a single walled carbon nanotube has a theoretical thermal conductivity of 6600 W/m K.[6] Experimental studies to confirm this value have been largely unsuccessful due to the limitations that will be discussed later.

Although carbon nanotubes have impressive thermal properties, using them to make useful thermal conducting materials has been ineffective due to large amounts of phonon scattering between the individual nanotubes and the matrix filler material. The carbon nanotubes have high internal phonon velocities, but when built into a large matrix of thousands of tubes with an epoxy to hold them together, the phonon boundary scattering effects reduces the material's overall thermal conductivity. It is thought that this is due to carbon nanotubes being too small and the inability to produce large lengths of tubes.[10] The short length and small diameters of carbon nanotubes give rise to huge amounts of surface area that when put into a matrix, provides too many interfaces where phonon scattering dominates. Yet, there is still hope for other carbon based materials. Producing carbon fibers with larger diameters and much longer lengths reduces the individual thermal properties of the fibers, but when placed into a matrix, the drastically reduced interfaces allow for a greater overall thermal conductivity.

1.3.1 Thermal Conductivity of Carbon Fibers

Carbon fibers, especially those which are highly graphitic, have been shown to have extremely high thermal conductivities making them well suited for use in thermal management of composites.[1] Carbon fibers may be produced from an organic precursor or by gas growth. Any fiber-like material that has high carbon content will produce a carbon fiber through heat treatment; however, most carbon fibers are produced either from polyacrylonitrile (PAN), rayon, or pitch.[11] Studies have been conducted on PAN, rayon, pitch, and vapor based fibers. This short review will serve to show how the thermal conductivities of these fibers compare with one another and can be seen graphically in Figure 5.

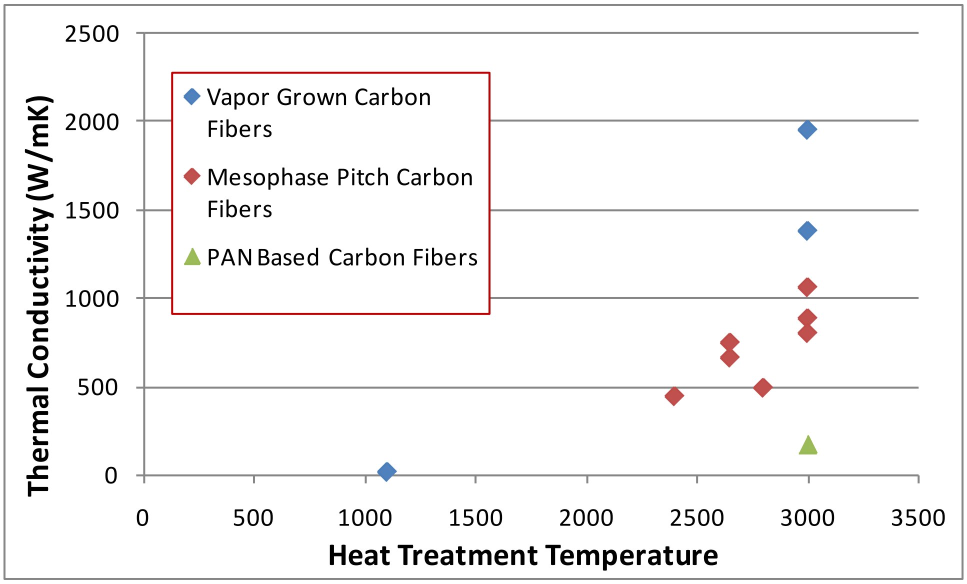

Figure 5: A review of thermal conductivity measurements on multiple types of carbon fibers. The thermal conductivity is plotted as a function of temperature to show how increasing the heat treatment temperature improves the thermal performance.

It has been shown over the past three decades by several authors that the thermal conductivity of carbon fibers can vary greatly depending the microstructure of the fiber.[1,7,12] Highly oriented pyrolytic graphite has a measured thermal conductivity of around 1950 W/m K at room temperature,[7] and carbon fibers may achieve this same performance if the fiber is composed entirely of graphite planes oriented axially. Vapor grown carbon fibers are the most thermally conductive carbon fibers due to their excellent structural perfection after heat treatment. This perfect graphite structure is the same as that in pyrolytic graphite. In 1984 Piraux et al. measured the thermal conductivity of vapor grown carbon fibers to be 1400 W/m K, remarkably high, but not quite as high as pyrolytic graphite.[7] One year later, Heremans et al. studied Pyrograf I vapor grown carbon fibers provided by Applied Sciences, Inc. and measured a thermal conductivity of 1950 W/m K, proving the perfect structure of these fibers after heat treatment. It is also interesting to see that Heremans measured the thermal conductivity of the fibers as grown to be only 20 W/m K. This value is the same as that of graphite measured through the planes, showing that as grown the planes align radially, but through graphitization at temperatures above 2400° C the planes reorient axially.[1]

PAN based carbon fibers generally have the lowest thermal conductivities of those studied, with a measured value of 175 W/m K by Piraux.[13] Carbon fibers produced from coal tar pitch are the most widely produced and studied of all fibers, and have displayed thermal conductivities from 123 W/m K to over 1000 W/m K depending on production methods and heat treatment, making comparisons among measurements and techniques very difficult.

Most pitch based carbon fibers have thermal conductivities between 440-800 W/m K with heat treatments between 2400° C and 3000° C. Finding studies of pitch based fibers with heat treatments below graphitization (2400° C) has not been possible, but it is expected that the thermal conductivity of these fibers will not change much before graphitization temperatures as the graphite planes will not reorient.[1] Gallego et al. studied a ribbon shaped carbon fiber heated only to the onset of graphitization and measured a thermal conductivity of 442 W/m K.[14] This value can be used as a good approximation for the thermal conductivity of an as grown mesophase pitch carbon fiber. A summary of all relevant thermal conductivity measurements can be seen graphically in Figure 7.

In Figure 7 it can also be seen that as carbon fibers are heated to higher temperatures their thermal conductivities tend to increase. This is due to graphitization, where carbon bonds are broken and reformed into ordered graphite planes. As these planes orient axially and defects are eliminated, the thermal conductivities continue to increase. Vapor grown carbon fibers are most thermally conductive due to their well ordered structure but are also the most expensive. PAN based fibers are the cheapest but are generally disordered keeping their thermal conductivities low even at high heat treatment temperatures.[13] Mesophase pitch based carbon fibers are also quite conductive, up to two times that of copper, and they are also readily available in large quantities. The drawback to using any of these fibers is the need to heat them to extremely high temperatures for graphitization, which substantially increases their cost. If a fiber is developed which has well oriented graphite planes at low heat treatment temperatures, cheaper thermal composites could be made.

Chapter 2 - Materials

Carbon fibers are complicated materials involving many stages in their processing and production, where small changes to any one step can greatly affect the properties of the fiber. Carbon fiber precursors are nearly unlimited in number, but the best fibers come from precursors with a well ordered structure. In the next several sections it will be shown how coal tar pitch, vapor grown, and electrospun fibers are produced. Typically the best quality fibers, especially in terms of thermal conduction, come from these processes which will be described in more detail below.

For this work, fibers are tested from each of the three groups previously listed. Commercially available melt spun carbon fibers from Mitsubishi were used to validate the testing method. These fibers are relatively easy to work with due to their microscale diameter and extremely long lengths. Vapor grown carbon fibers, formally known as Pyrograf I, were obtained from Applied Sciences Incorporated. These fibers exhibit an extremely high thermal conductivity due to their highly ordered graphite structure obtained from their production method. Lastly, the University of Akron provided electrospun polyimide fibers with the addition of coal tar pitch. The pitch was added in varying percentages in order to study how the fibers thermal conductivity changes as a function of pitch content. Working with collaborators from the University of Akron several attempts were made at how to deposit and manipulate these fibers. Initial attempts focused on depositing fibers directly onto an SEM stage for testing, but finally an alternate deposition method requiring more manipulation was chosen. All of these materials as well as how they were handled and used will be described subsequently.

2.1 Synthesis of Melt Spun Carbon Fibers

Melt spun carbon fibers have been produced for many decades and now make up a large bulk of the carbon fiber industry. These fibers have high performance and are not extremely expensive or difficult to produce. Melt spun fibers are produced from coal tar pitch precursors, although many forms and compositions exist. Coal tar pitch has a very complex structure and chemical composition that is a mixture of fused ring aromatic compounds with alkyl side-chains and heterocyclic compounds. The properties of a certain pitch, and hence the fibers produced with it, depend on its chemical composition and molecular weight distribution.[12] Typically these pitch based fibers are produced using melt spinning techniques and fall into two categories, general purpose and high performance carbon fibers. The difference between these two groups of fibers is a result of the type of pitch used. General purpose carbon fibers are produced using an isotropic pitch, whereas high performance fibers are made using mesophase pitch. The use of mesophase pitch (liquid crystal) allows the structure of the final fiber to be more oriented and more graphitic than isotropic fibers, which results in stronger, more thermally conductive fibers, thus making them the focus of this thesis.[11,12]

The first step to producing a pitch suitable for carbon fiber production is the removal of impurities that purify and modify the pitch allowing it to be melt spun. Mesophase pitches are able to be melt spun because the pitch softens and melts below its degradation temperature. There are many different ways that pitch is modified to achieve the desired processability, including thermal polymerization, solvent extraction, catalyst modification, and hydrogenation.[11] Each of these techniques attempts to create an easy-to-spin carbon fiber, and each has its advantages and disadvantages. Mitsubishi Chemical uses the catalyst modification method to produce their carbon fibers, resulting in a pitch with a very narrow range of molecular weights.[15] After taking one of these necessary steps to prepare mesophase pitch for production, melt spinning of the carbon fibers can proceed.

Melt spinning begins with the mesophase pitch being loaded into the hopper of an extruder as solid chips as shown in Figure 6.[12] A rotating screw in the extruder moves the chips toward the melting section, where the pitch begins to soften and melt. As the melted pitch is pushed along, it enters an increasingly narrow region where the fluid's pressure builds. The melted pitch is then forced into what is known as the metering pump, whose sole purpose is to reduce pressure variations within the molten pitch. After the metering pump, the pitch enters the spin pack, which contains a filter to remove any small particles not removed in previous processing steps. Finally, the pitch is forced through the spinneret, a plate with very small holes in it, to create the carbon fiber strands. As the strands exit the spinneret the surrounding atmosphere quickly cools the pitch to create solid carbon fibers, which can then be wound up on a rotating wheel or collected on a conveyor belt. Although melt spinning seems like an easy process, it is actually very complicated, and very small changes in anything from the processing conditions to the size of the holes on the spinnerette can completely change the properties of the carbon fiber.[12]

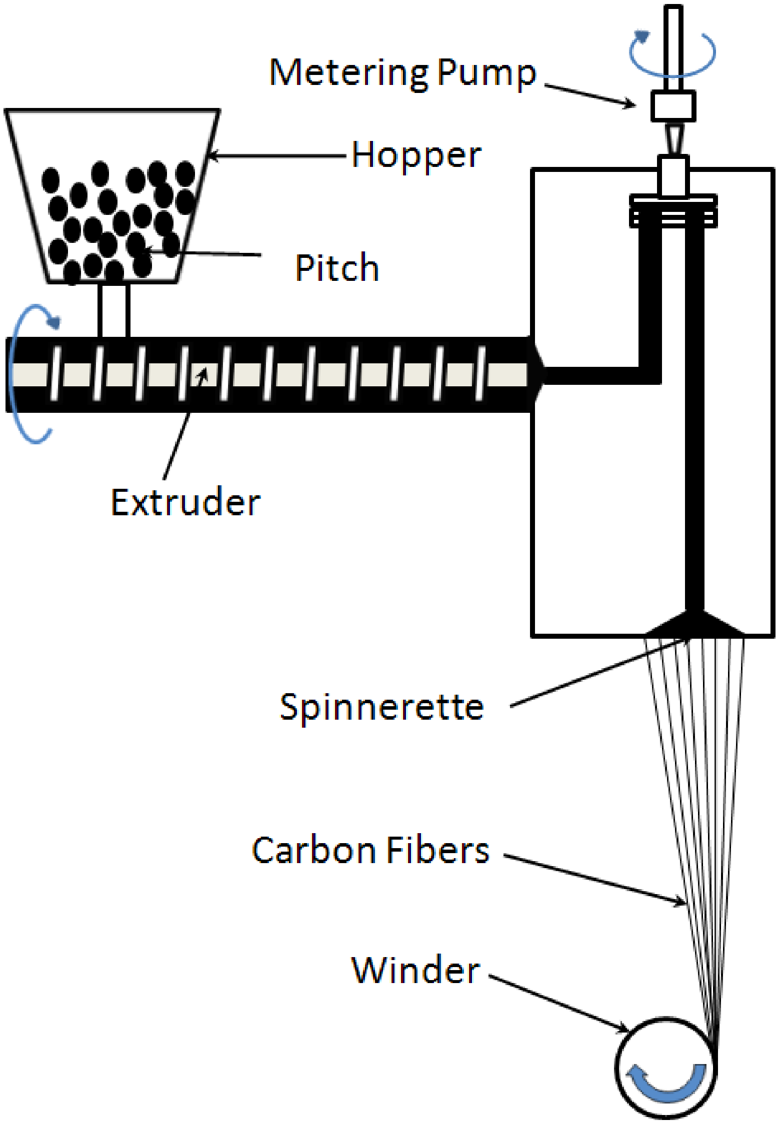

Figure 6: A melt spinning apparatus for the production of carbon fibers.

The as-spun carbon fibers are a thermal plastic material that must be thermoset to prevent future melting and thermal relaxation. However, to convert the fibers from a thermoplastic to a thermoset material, oxidation of the fibers is necessary. Thus, most carbon fibers can be exposed to air at 230-280 degrees Celsius to provide oxidative stabilization.[12] Following the stabilization procedure, carbon fibers can go through several more post-production steps to alter their physical properties. Carbonization is typically employed at temperatures below 2000 degrees Celsius in an inert atmosphere to remove most non-carbon elements, in an effort to enhance the physical properties of the fibers. Further heat treatment such as graphitization can be conducted at temperature up to 4500 degrees Celsius to improve the degree of preferred orientation within the fiber for higher elastic modulus and thermal conductivity.[11]

The fibers obtained from Mitsubishi are known as DIALEAD K13D2U carbon fibers. The specifics of their production is not readily available, however it can be assumed that they are produced quite similarly as described above. The exact coal tar pitch used in their production is not known, but is likely a mesophase pitch, which leads to the fibers relatively high thermal conductivity of 800 W/m K.[15] After speaking with Mike Rainaldi, director of Mitsubishi Chemical FP America, it was learned that these specific fibers are heat treated to just over 3000 degrees Celsius. The fibers used for this study were all about 11 microns in diameter and had individual lengths of over 10 centimeters.

2.2 Synthesis of Vapor Grown Carbon Fibers

Vapor grown carbon fibers (VGCFs) are a new class of carbon fiber produced through the pyrolysis of a hydrocarbon containing gas in a hydrogen containing atmosphere at elevated temperature. The hydrocarbons break down and reform on ultra-fine transition metal catalyst particles such as nickel, iron, or cobalt. These catalyst particles can either be seeded directly onto a substrate such as silicon or quartz (fixed catalyst method) or injected directly into the gas (floating catalyst method).[13] The fibers used in this study were produced using the fixed catalyst method and methane was used as the carbon source. VGCFs have been shown to exhibit the highly preferred orientation of the graphitic basal planes parallel to the fiber's axis with an annular ring texture in the cross section. This well oriented structure gives rise to very good mechanical, electrical, and thermal properties, especially after further processing such as carbonization and graphitization.[11]

The vapor grown carbon fibers tested in this work were provided by Applied Sciences Inc. and are known as Pyrograf I carbon fibers. These fibers are gas grown and range between 3 and 20 microns in diameter; those used in this study were generally around 5 or 6 microns. The fibers are grown at an elevated temperature around 1100˚ C and are then heat treated to over 3000˚ C. According to a paper by Heremans et al., these fibers have an as-grown thermal conductivity of about 20 W/m K and a heat treated thermal conductivity of about 1950 W/m K.[1]

These fibers come in two varieties, those which grow below the substrate and those which grow above. The fibers which grow below are known as short staple and those obtained from ASI were typically less than two centimeters long. The short staple fibers are quite easy to separate but are not quite the ideal length for testing. Those which grow above the substrate are grown in “forests” with little to no spacing between fibers. These forests are over seven centimeters in length and were provided as mats of fibers all oriented along one plane as shown in Figure 7.

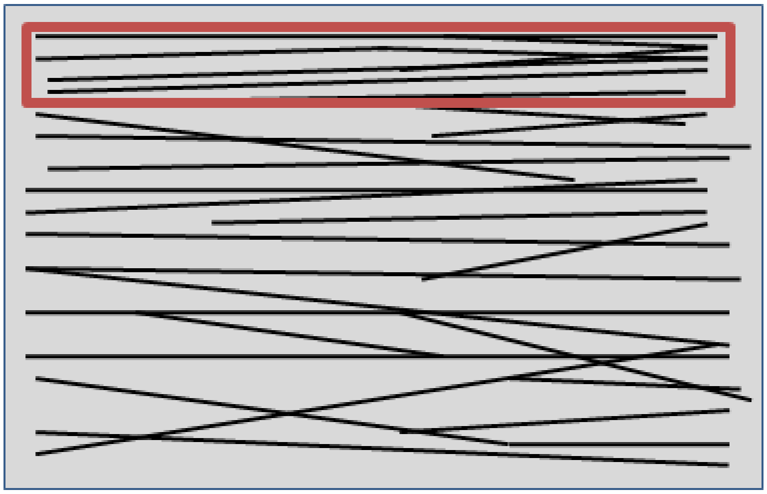

Figure 7: This is a representation of a mat of Pyrograf I fibers. In actuality the fibers are spaced much closer together but here they are spaced far apart to emphasize the structure. The red box highlights an area within the mat where fibers are very well aligned and a bundle for testing would be taken.

Separation of individual fibers from these mats is possible, but not while maintaining the long lengths necessary for testing. Instead, removal of very long and narrow sections make up of about a dozen fibers proved much more successful and is thus used for testing these fibers.

2.3 Electrospinning of Polyimide

Electrospinning is a process used for the production of polymer fibers using electrostatic force. Typically a pipette is used to hold a polymer solution, and a DC power supply is used to create a strong electric field between the pipette and a collection plate. When a sufficiently high voltage is applied, the electrical forces at the surface of the polymer overcome surface tension, and an electrically charged jet is ejected, as depicted in Figure 8. The polymer chains are entangled within the jet, preventing it from being broken apart as it travels toward the collection plate. The charge in the jet causes the fiber to spin as it travels, and with each revolution the diameter of the fiber decreases. There are essentially two ways to electrospin fibers: using a polymeric solution or using a polymer melt. When working with a polymeric solution, the solvent used to dissolve the polymer must evaporate as the fiber reaches the collection plate, allowing the polymer to solidify. When using a polymer melt, the jet cools as it travels and finally solidifies as it reaches the collection plate.[16]

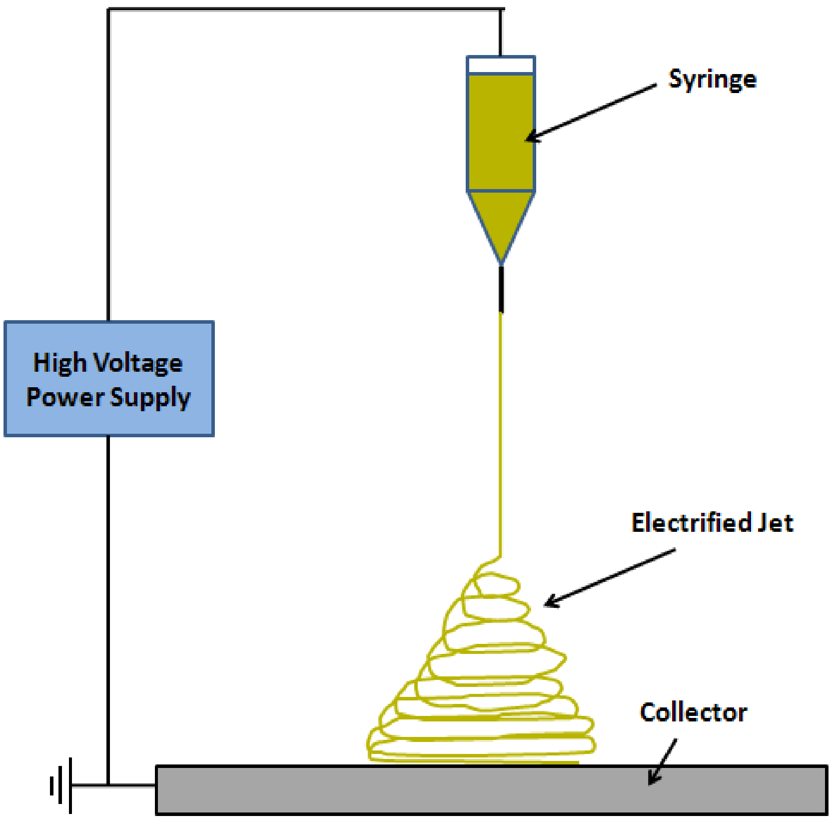

Figure 8: This graphic depicts the electrospinning apparatus. The solution to be spun is placed inside the syringe, and a high voltage power supply creates a strong electrical field to draw the solution toward the collector.

Electrospinning can be applied to many different polymers, but the work of this thesis focuses on the electrospinning of poly(amic acid), for the production of polyimide fibers. Polyimides are typically very chemically stable, making their dissolution in a solvent very difficult, and thus not suitable for being electrospun as a solution. Polyimides also decompose prior to melting, thus making them not suitable to being spun as a melt.[17] Therefore, polyimide fibers are generally prepared by electrospinning poly(amic acid) (PAA) precursors dissolved in polar solvents.[18] The typical procedure for producing polyimide fibers contains three steps:

1. Forming a PAA precursor – Copolymerizing the necessary precursors in an appropriate solvent to create a PAA solution[18]
2. Electrospinning the PAA – Using high voltages to draw an electrically charged jet from a pipette down onto a collection plate[18]
3. Converting the PAA to polyimide – Step heating of the PAA electrospun fibers up to 350-400 degrees Celsius to thermally convert PAA to polyimide fibers in a process known as imidization[18]

Electrospinning is a fast, simple, and relatively inexpensive process that can produce very long and thin fibers, which is why it was used in this study.[16]

Although the technique outlined here is for producing pure polyimide fibers, this process has been modified by collaborators at the University of Akron to allow spinning of polyimide fibers with added mesophase pitch. By choosing an appropriate solvent, certain weight percentages of coal tar pitch can be added and dissolved in the PAA solution and still be suitable for electrospinning. By electrospinning these fibers, the polyimide merely acts as a carrier for the pitch, allowing it to be electrospun. Professor Cakmak and his student Han Yan have been generous enough to provide these fibers for thermal testing.

The fibers were solution spun from a mix of Dupont HE polyamic acid and ground flakes of coal tar pitch dissolved with a strong solvent. The solution was then spun into fibers directly onto aluminum foil that was folded into a saw tooth pattern, as shown in Figure 9.

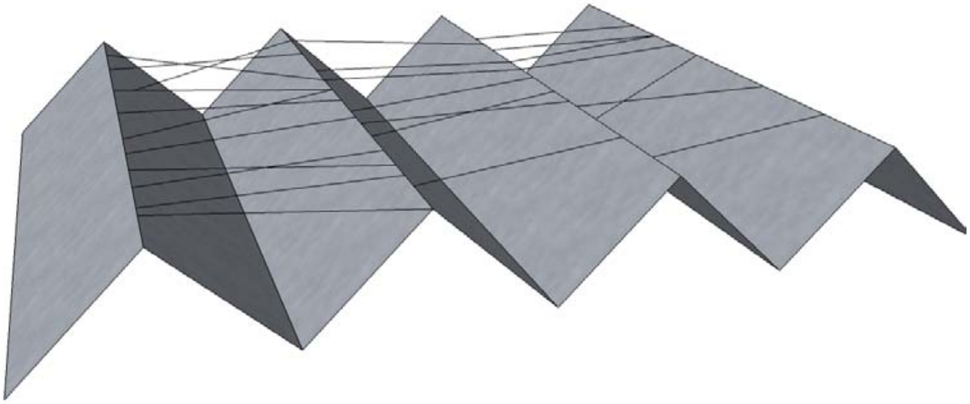

Figure 9: Representation of the saw tooth shaped aluminum foil upon which the composite fibers are electrospun. The electrical fields are greatest at the peaks of the foil causing the wires to align perpendicular to them.

The shape of the foil allows the fibers to be suspended, and also controls the fibers alignment. The sharp corners produced by folding the foil causes strong electrical fields to emanate from these points. When the fibers are spun, they move in response to these fields and align perpendicular to the folds. This deposition process also allows the fibers to remain suspended for easier manipulation. After spinning, the fibers must be thermally imidized through step heating up to 400 degrees Celsius. This imidization procedure converts the polyamic acid into polyimide making the fibers much more stable. The fibers are typically around two centimeters in length and vary in diameter from 100 to 500 nanometers.

2.4 Fiber Positioning

The most challenging aspect of the method is suspending a fiber across the SEM stage for testing. Essentially the test stage is a square plate with a wide groove cut from the middle. A sensor exists on one raised end of the stage and an insulating support sits on the other. Each fiber tested must be precisely placed to only contact the sensor and insulating support, while suspended above the groove so that a heater may easily be positioned underneath it. Many of the techniques needed to properly manipulate the fibers into proper position depend on the fiber being tested. For example, micron sized fibers can be seen and thus moved about without the naked eye, while nanometer scaled fibers need to be placed on the sensor under a light microscope or electron microscope, if necessary.

The key to obtaining a good measurement with this method is achieving a proper contact between the fiber and sensor. This junction is very important because the heat must move through the fiber and into the sensor relatively unobstructed. Although the thermal contact resistance at this junction does not need to be known in order to make a correct measurement, in order to generate sufficient heating of the sensor a good thermal contact must exist at this point. More importantly than a good thermal contact, the fiber should not move during testing. This seems obvious but when testing stiff, large diameter fibers such as coal tar pitch carbon fibers, any slight contact between the heater and fiber will cause some movement of the fiber on the sensor. This results in non-localized heating of the sensor producing long sloping voltage changes rather than an exponential rise. In summary, when placing fibers, they should have good thermal contact with the sensor and be held strongly in place as not to move when contacted by the heater.

Chapter 3 – Experimental Methods

Current methods for testing the thermal properties of micro and nano structures are limited in their use due to experimental errors as well as unnecessary complexities. By studying these techniques, a more effective method for rapidly measuring the properties of a wide range of materials could be developed. Before introducing the technique employed for this work, a review of important methods previously used for measuring thermal properties of micro and nanostructures will be outlined, and their shortfalls will be examined to explain the need and process used to develop the thermal flash method.

3.1 Previous Micro/Nano Thermal Characterization Techniques

For more than two decades people have been attempting to characterize the thermal properties of micro and nano structures. In the 1980s people focused research on individual carbon filaments with diameters in the microns, and much more recently people have been able to characterize the thermal properties of individual nanostructures. The techniques used for these measurements can be split into two groups, steady-state and transient measurements. There are advantages and disadvantages to using both, although steady-state techniques seem to be much more common.

3.1.1 Steady-State Techniques

Steady-state measurement techniques all involve the same three steps: adding heat to a system, waiting until the system stabilizes, and then measuring how the heat flows. The most basic of these techniques is commonly referred to as the heat flow meter and continues to be used today. The heat flow meter is essentially a heater at one end of a sample and a heat sink at the other end with temperature measurements taken along the length of the sample as shown in Figure 10. By examining how the heat diffuses through the sample a thermal conductivity can be found. Similar techniques were used by several authors, such as Piraux et al. and Heremans et al., to measure the thermal conductivities of different types of carbon fibers in the 1980's.[1,7] Recently, May et al. used this technique to measure the properties of Diamond/Tungsten fibers.[19] This technique is very difficult to use with small diameter fibers because the use of thermocouples to measure temperature becomes impossible.

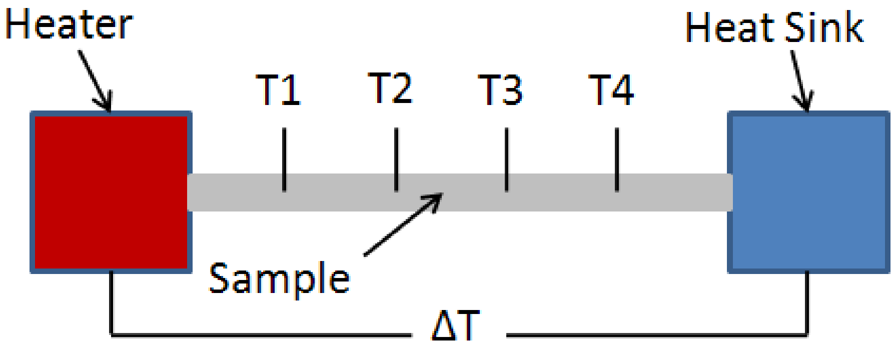

Figure 10: The heat flow meter for measuring thermal conductivity.

The first group to successfully measure the thermal conductivity of a single carbon nanotube was Kim et al. in 2001.[20] They used a microfabricated setup consisting of a heater at one end and a sensor at the other, between which a carbon nanotube was suspended as in Figure 11. This setup is exactly the same as a heat flow meter arrangement, although the small size of the carbon nanotube prevented them from directly measuring the temperature drop across the tube. Instead, they measured the temperature difference between the heater and sensor using two resistors and used this as an estimate of the thermal conductivity of the tube. By not measuring the temperature along the tube, and instead measuring it from pad to pad, much higher error is introduced due to thermal contact resistances between the tube and the heater and the tube and the sensor. This reduces the amount of heat the tube can transport. Unfortunately these uncertainties are nearly impossible to estimate and thus lead to incorrect measurements.

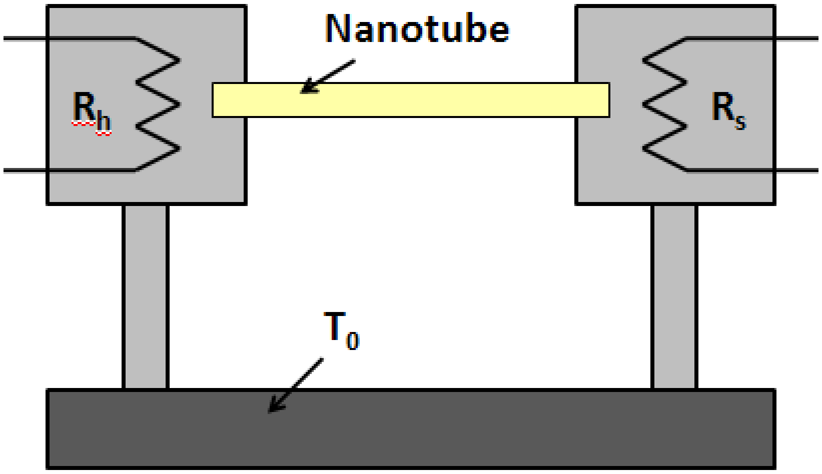

Figure 11: The experimental configuration described by Kim for measuring the thermal conductivity of a carbon nanotube.

A different technique relying on similar steady state principles was derived by Zhang et al. in 2000.[21] In this hot wire method a small current is passed through a platinum wire to induce uniform heating of the wire. A base temperature profile is established by measuring the current and voltage needed to heat the wire. Next, the fiber to be tested is placed in the middle of the heated wire and extends to a heat sink as shown in Figure 10. The fiber draws heat out of the hot wire and passes it to the heat sink, causing a significant temperature reduction in the hot wire. The voltage and current required to maintain heating is compared to that before the fiber was added in order to measure the fibers thermal conductivity. This method does not account for contact resistances that occur between the fiber and hot wire and the fiber and the heat sink, both of which cause some uncertainty in the measurements.

The hot wire method was adopted by Fujii et al. in 2005 to measure the thermal conductivity of carbon nanotubes.[22] In this experiment, a device was microfabricated consisting of a hot wire sensor and heat sink as shown in Figure 12. The experiment consisted of two parts just like the hot wire method. The first baseline measurement was conducted with no nanotube suspended between the hot wire and the heat sink, while the second part had the suspended tube. By comparing the measured voltages between the first and second parts of the test, the thermal conductivity of the nanotube was determined. This method again has no way to account for thermal resistances, and a lack of measurement sensitivity prevented this method from being used on tubes of small diameter. Later, Dames et al. used the same method but deposited tungsten at the junction between the nanotube and the hot wire in order to reduce the thermal and electrical contact resistances.[23] Very recently in 2009, Wang et al. determined a way to measure the thermal contact resistance at the fiber/hot wire junction by using different fiber lengths.[24] Although this method finally does eliminate the effect of thermal contact resistance it is very time consuming because of the need to measure several fiber lengths in order to make one complete measurement.

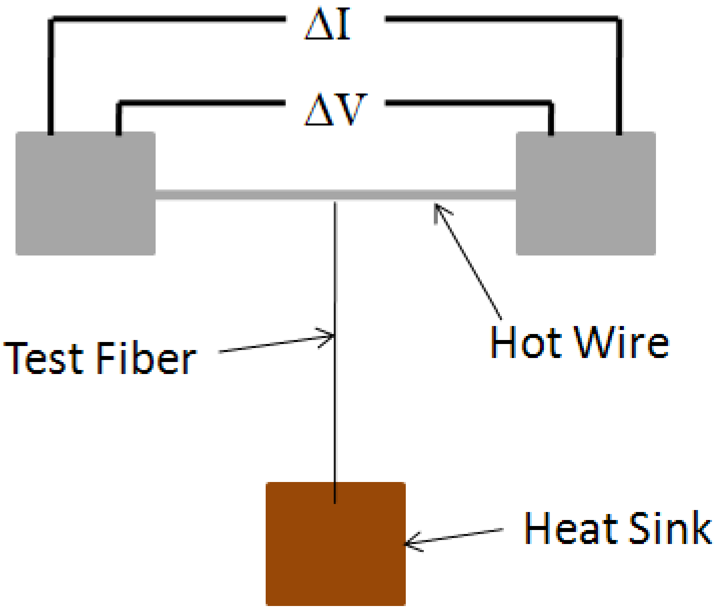

Figure 12: T-type sensor used for nanotube thermal conductivity measurements. A fixed current is passed through the heater, and the voltage across the heater measured, both with and without a nanotube present in the system. The change in resistance of the heater is related to the heat drawn out of the system through the nanotube, which in turn depends on the nanotube thermal conductivity.

Other notable steady state measurements include the 3-omega technique and the thermoreflectance technique. The three omega method was developed by Cahill in 1990,[25] and was adopted by Choi et al. in 2005 to measure the thermal conductivity of carbon nanotubes.[26] This method also uses a microfabricated device composed of four separate pads across which a nanowire is placed, shown in Figure 13. An AC current is fed across the two outside pads at the first harmonic which induces heating in the nanotube at the second harmonic. This heating of the tube generates a change in resistance that induces a voltage difference between the middle two pads at the third harmonic. This third harmonic voltage is related to the thermal properties of the tube and is thus used to calculate the thermal conductivity or diffusivity. Thermal resistances do not matter in this experiment because they only lower the amplitude of the signal but not the frequency. However, by dealing with these three harmonic frequencies, the complexity of the experiment is greatly increased.

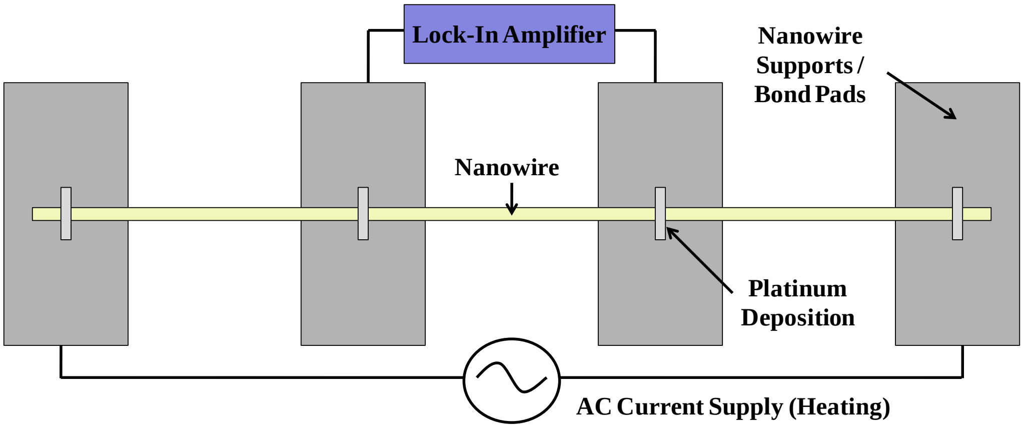

Figure 13: Here is the three omega experimental configuration used by Choi et al. to measure the thermal conductivity of a carbon nanotube.

The thermoreflectance technique was developed by Zhang et al. in 2006 to measure thermal properties of silicon nanowires.[27] The microfabricated device used for this measurement was very similar to that of Kim et al.,[20] and consisted of two pads between which a nanowire was placed. One of the pads had a voltage bias across it in order to generate heating, from which part would flow across the nanowire and into the other pad. The temperatures of the two pads were compared in order to calculate the thermal conductivity of the nanowire. Again there was no way to account for contact resistances between the pads and the nanowire so this method may not have reported accurate measurements.

The above methods all rely on steady-state conduction to make thermal conductivity measurements, but thermal contact resistances inevitably add error to these techniques. Some of the steady-state techniques have found ways to determine the contact resistances but these techniques are very time consuming to perform. In efforts to eliminate thermal contact resistances several transient techniques were developed to measure thermal diffusivity, but these methods introduce other complications.

3.1.2 Transient Techniques

Transient measurement techniques are far less common than steady state methods and the first ones discussed in this section were only published in 2006. Huo *et al.* developed the optical heating and electrical thermal sensing (OHETS) method in 2006 for measuring thermal properties of individual micro and nanostructures.[28] In this experiment, a wire is suspended between two electrodes as shown in Figure 14. A constant DC current is applied across the wire and voltage drop through the wire is measured. A periodically modulated laser beam then shines over the entire wire, causing temperature variations within the wire, thus resulting in periodic changes in the electrical resistance of the wire. These resistance changes then cause voltage changes across the wire. By examining the phase differences between the periodic heating from the laser and the periodic voltage changes, thermal conductivity of the wire can be found. This method therefore only works on electrically conductive materials that will generate appreciable resistance changes with temperature.

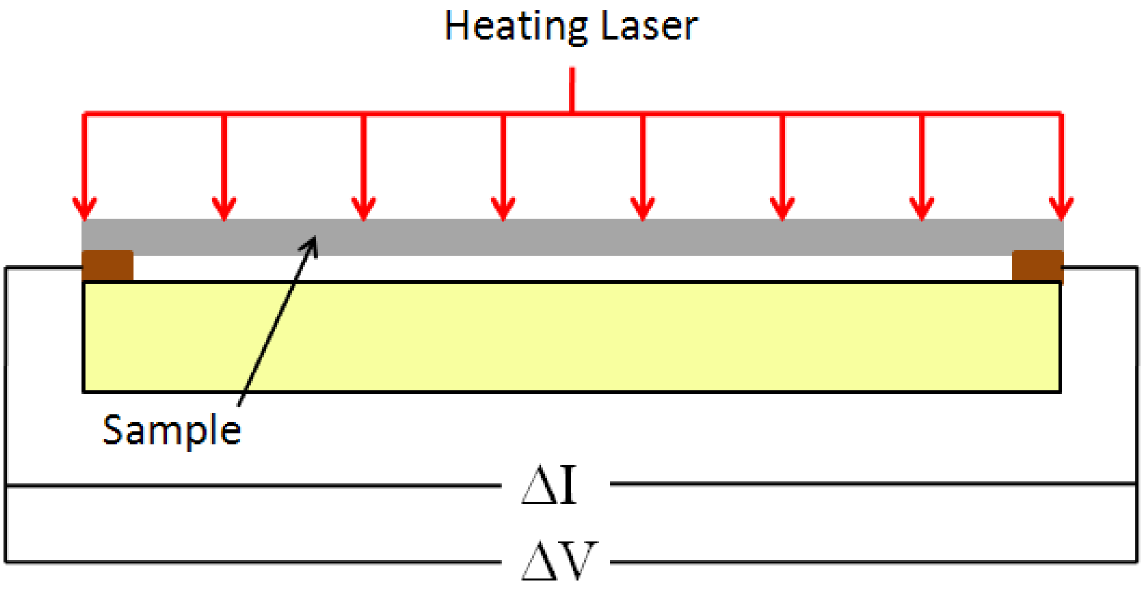

Figure 14: The OHETS and TPET methods for thermal diffusivity measurement. The OHETS method uses a modulated laser beam, and the TPET method uses a single transient caused by switching the laser on.

A slight variation on the OHETS method is the transient photon-electro-thermal (TPET) technique proposed by Wang *et al.* in 2007.[29] For this method a DC current is also passed through a wire suspended between two electrodes. Instead of using a periodically modulated laser to generate temperature changes in the wire, this method uses the initial transient caused by switching the laser on. This causes the electrical resistance of the wire to change with time, and the resulting change in voltage across the wire is measured as a function of time. The temperature response is used to extract the wire's thermal diffusivity. Although this is a simpler transient method, it still requires the use of an electrically conductive wire which will generate an appreciable resistance change with temperature.

Another very similar technique for characterizing the thermal properties of micro/nanowires is the transient electrothermal technique (TET) developed by Guo *et al.* in 2006, and shown in Figure 15.[30] Here a wire is also suspended between two electrodes, but instead of using a laser to heat the wire, a direct current is passed through the wire to create heating. As the wire heats up, its resistance changes, and the transient voltage response of the wire is measured as a function of time. The measured voltage is then compared to the analytical solution to calculate the material's thermal diffusivity. This method has very similar limitations to that of the OHETS method, as the two methods are nearly identical. An electrically conductive wire must be used for the TET method which will generate enough of a resistance change to allow for a measurable voltage change. However, this method was later applied to non-conductive polymer wires by depositing a thin gold coating to the top of the wire.[31] This coating acts as both a heater and a temperature sensor allowing the use of non-conductive wires, however, the gold deposition complicates the measurement, and because metallic deposition is not possible on the nanoscale, this method is limited to use with microscaled wires.

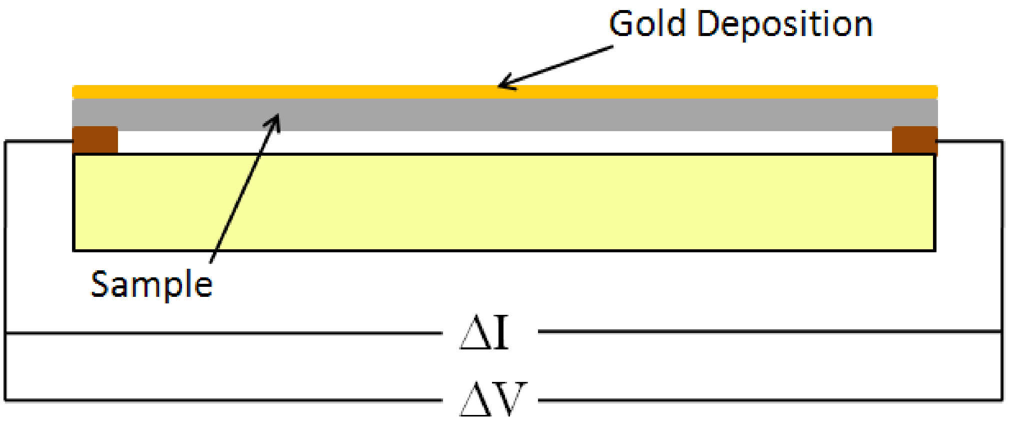

Figure 15: The TET method for thermal diffusivity measurement.

The steady-state techniques described above have either too much error due to thermal contact resistances or are much too difficult to perform. Transient techniques seem to be a better choice because of the elimination of thermal contact resistances and faster processing. However, they only measure thermal diffusivity, thus requiring knowledge of the material's density and specific heat to calculate thermal conductivity. The transient techniques seem to generally be too limited in scope, i.e. only for use with electrically conductive wires, or far too difficult for rapid and simple testing. Many of these methods also depend on the need for microfabrication which is both difficult and costly. For these reasons a novel technique was developed to attempt to eliminate complications caused by previous methods.

For this work, a transient technique is chosen to avoid thermal contact resistances with the two main goals being a simple and rapid thermal characterization method. The "thermal flash method," initially developed in the nanoEngineering laboratory at CWRU, is improved to characterize both micro and nanoscaled materials and to work with electrical insulators as well as conductors. The technique was first developed by Demko and Abramson for low thermal diffusivity materials and is now being adopted for use with high thermal diffusivity samples.[32]

In an effort to improve upon previous techniques, a simple and efficient method for measuring the thermal diffusivity of highly conductive fibers has been developed for use within a scanning electron microscope (SEM). Loosely based on the laser flash method, this transient thermal flash technique uses a micromanipulator based heater to send a heat pulse through a fiber and into a sensor. The thermal response of the sensor causes a transient electrical resistance change that is used to determine the thermal diffusivity of the fiber. A rather simplified technique has been developed where thermal contact resistance does not affect the result. This technique has previously been validated for low diffusivity materials by measuring the properties of both glass and polyimide micro/nanofibers. In order to confirm the accuracy of this method for high diffusivity fibers, initial testing was performed on Mitsubishi K13D2U carbon fibers. Later, testing was expanded to other carbon micro/nanomaterials such as VGCFs and polyimide with mesophase pitch fibers.

3.2 Analytical Solution

The thermal flash technique is based off one dimensional heat conduction from a heater through the fiber being tested and into a thermal sensor. Based on how fast heat moves through the fiber to the sensor, the fiber's thermal diffusivity may be found. In order to solve for the thermal diffusivity an analytical solution for the temperature rise of the sensor must be found as a function of the thermal diffusivity of the fiber.

To determine the temperature rise of the sensor without the use of a numerical simulation, an analytical solution is needed. This solution is based on 1D heat conduction that an appropriate experimental setup mimics. A solution is found for a 1D heat conduction problem through two materials with constant temperature at one end and a constant higher temperature at the other end with a heat flux condition in the middle. This setup is shown in Figure 16, and an analytical solution exists for this situation. Here the left end of the model is the point on the micro/nanowire that is contacted by the heater. The temperature at this point, T_r, is assumed to instantly rise to that of the heater and not change during a measurement. The far end at T_0 is the contact between the aluminum wire bond sensor and the copper heat sinks. This point is assumed to stay at ambient temperatures during testing because the heat sinks are very large compared to the test sample and sensor. In the middle it is assumed that an intimate contact exists between the fiber being tested and the aluminum sensor. The temperature at this point is unknown, and needs to be solved for. It is assumed that a constant heat flux condition exists at this point; any heat leaving the end of the test fiber must flow into the sensor.

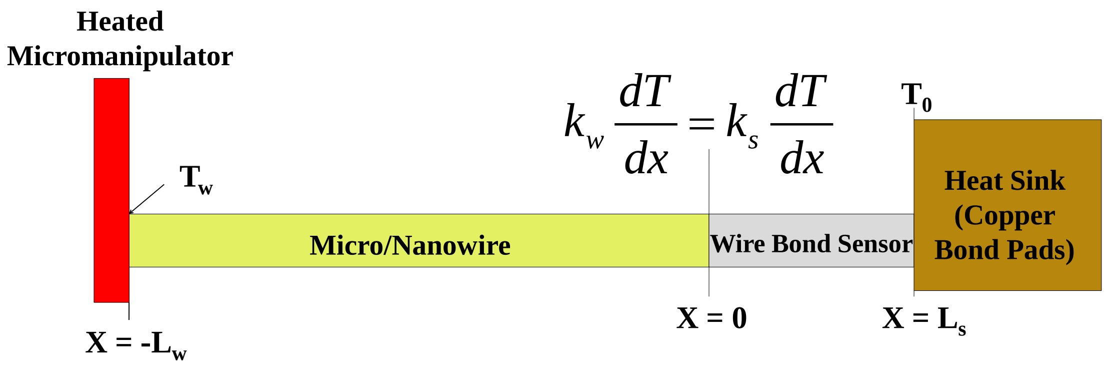

Figure 16: This is an illustration of the experimental configuration which was used for the analytical solution. The system is modeled as a 1D heat conduction problem with constant temperature ends.

Although an analytical solution was found for our setup, all the assumptions need to be verified. For this purpose, a numerical finite-difference model was coded to verify that no mistakes were made. The assumption that the point on the wire where the manipulator touches instantly jumps to a higher, constant temperature is valid because the diameter of the wires tested using this method are much smaller than the diameter of the micromanipulator. The heat sink was also designed to be much larger than the sensor and the wires being tested, so the assumption that its temperature will not change is also valid.

Convection effects were neglected because the entire setup is placed under vacuum in an SEM. Thermal radiation will still exist, especially from the heater to the walls of the SEM. This radiation will cause only very minimal temperature rises in the sensor and fiber due to their small size and the relatively low temperature of the heater. Radiation effects during a measurement were neglected since over the short period of time needed to measure a rise time, generally about 0.3 seconds, radiation loses are minimal. Also, even if thermal radiation losses are large, this would affect the magnitude of the exponential and not its shape, causing no influence on the measurement. Again, because only the shape of the temperature curve, and not its magnitude, is needed to find the thermal diffusivity of the wire, any thermal contact resistances will have no effect on the solution.

Using the one dimensional model from Figure 16 the temperature of the sensor may be solved as a function of time. The complete derivation of this equation can be found in appendix A1. The temperature rise of the sensor for the setup shown in Figure 16 is mathematically displayed as:

$$\begin{aligned} T_s &= T_0 + \frac{\Delta T\, k_w\, l_s}{k_w l_s + k_s l_w} \\ &- 2\,\Delta T \sum_{m=1}^{\infty} \frac{\sin \alpha\beta_m l_s \cdot\, e^{-\alpha_w \beta_m^2 t}}{\beta_m\{(l_w + \sigma\alpha l_s)\sin\beta_m l_w \sin\alpha l_s\beta_m - (\sigma l_w + \alpha l_s)\cos\beta_m l_w \cos\alpha l_s\beta_m\}} \end{aligned} \tag{3.1}$$

T_s = Sensor Temperature	T_w = Wire Temperature
α_s = Sensor Thermal Diffusivity	α_w = Wire Thermal Diffusivity
l_s = Sensor Length	l_w = Wire Length
k_s = Sensor Thermal Conductivity	k_w = Sensor Thermal Conductivity
T_0 = Ambient Temperature	ΔT = Temperature Difference between Manipulator and Heat Sink
$\alpha = \sqrt{\frac{\alpha_w}{\alpha_s}}$	$\sigma = \frac{k_s}{k_w}\alpha$

The values of β in the equation for the sensor's temperature come from the solution of the transcendental equation:

$$\cos \beta l_w \sin \alpha\beta l_s + \sigma \sin \beta l_w \cos \alpha\beta l_s = 0 \tag{3.2}$$

The equation for the sensor's temperature is rather complicated and in an effort to simplify it, a few assumptions may be made. The simplifications stem from the transcendental equation used to solve for β. When measuring a high thermal diffusivity micro/nanowire, the length of the wire needs to be very long in order to obtain the correct rise time. Because of this we can make the assumption that:

$$l_w \gg \propto l_s \tag{3.3}$$

This assumption means that in equation 3.2 the sinusoids containing βl_w will be much higher frequency than those containing $\alpha\beta l_s$. When finding the first several zeroes when solving for β it can be assumed that the $\alpha\beta l_s$ sinusoids are small to the point that the small-angle approximation can be applied. In this way, equation 3.2 simplifies to:

$$\alpha\beta l_s \cos \beta l_w + \sigma \sin \beta l_w = 0 \tag{3.4}$$

From this equation it is clear that a relation between σ and $\alpha\beta l_s$ could be useful. By examining equation 3.4 it can be seen that β should have a magnitude on the order of $\frac{n}{l_w}$. Also, as assumed previously in equation 3.3, αl_s should be small compared to l_w, so the quantity $\alpha\beta l_s$ should be small compared to σ assuming β is not extremely large.

After plugging in the order of magnitude for β the second simplifying assumption can be expressed as:

$$\frac{k_s}{k_w} \gg \frac{nl_s}{l_w} \tag{3.5}$$

Finally the transcendental equation and β may be expressed as:

$$\sin \beta l_w = 0 \tag{3.6}$$

$$\beta = \frac{n\pi}{l_w} \tag{3.7}$$

Utilizing the solution of β as well as the two simplifying assumptions (Equations 3.3 and 3.5) the expression for the temperature of the sensor may be simplified. This simplification was done in Mathematica and a complete derivation follows in the appendix. After plugging in our value of β and using our assumptions, any terms dealing with the magnitude of the temperature may be dropped, leaving this rather simple elliptic theta function:

$$T_s(t) = 1 + 2\sum_{n=1}^{N}(-1)^n e^{\frac{-n^2\pi^2 t\alpha_w}{l_w{}^2}} \ ,\ t > 0 \tag{3.8}$$

$$N \ll \frac{l_w k_s}{l_s k_w \pi} \tag{3.9}$$

This value of N comes from the first assumption. Because the value n appears in that assumption, the sum can no longer be infinite and must only go to N as defined by 3.9.

Using this simplified expression for the temperature of the sensor, a numerical fitting procedure was created to fit the experimental data to this analytical solution. It should be noted that this equation now only depends on the length of the wire being measured and the thermal diffusivity of the wire.

3.3 Data Analysis

Using the analytical solution detailed above the thermal diffusivity of the test material can be found from the temperature rise of the sensor. It is not feasible to measure the temperature rise of the sensor but as the sensor's temperature rises, its resistance will rise at the same rate, thus changing the measured voltage at the same rate. The temperature of the sensor must then be matched to the voltage change to find the thermal diffusivity. Because the process to find the thermal diffusivity involves matching two curves, a numerical program was developed to fit the temperature rise of the sensor to the measured voltage data. The program first normalizes the input voltage data because only the shapes of the voltage and temperature curves are important. An initial guess at the thermal diffusivity as well as the length of the measured wire must be input in order for the program to plot a first guess of the temperature rise of the sensor. The program then changes the thermal diffusivity of the wire and the start point of the exponential rise until the sum of the least squares error between the experimental voltage data and analytical temperature data is minimized. The thermal diffusivity that provides a best fit is given as the thermal diffusivity of the measured material.

As with all transient techniques, the thermal flash method measures thermal diffusivity of the fibers and not thermal conductivity. Although both provide information about a materials capability to conduct heat, thermal conduction is the more accepted measurement. In order to convert measured values from thermal diffusivity to thermal conductivity, equation 1.2 must be used, therefore the density and specific heat of the sample must be known. This information is not always available or easy to measure, especially for experimental materials.

3.4 Sensor Design

Based on the analytical solution and one dimensional conduction described above, an experiment needed to be constructed and a proper sensor was needed. Measuring the temperature of the sensor directly is not feasible due to its small scale, so instead, a metallic sensor is used which acts as a resistor. A small current is continuously passed over the sensor and the voltage drop is measured. As the metal heats up due to thermal conduction through the fiber, the resistance of the sensor changes. The resistance increase of the sensor causes the measured voltage to change. This voltage change has exponential shape, exactly the same as the sensor's temperature rise because a metals resistance is linearly dependent on temperature.

The key to the thermal flash method is the use of an appropriate sensor to provide a strong voltage change with temperature. In previous work, a sensor built at the University of Illinois was employed.[32] This sensor was microfabricated from a silicon wafer, and had a small tip approximately eight microns long, over which a wire was laid.

The sensor worked well for low diffusivity measurements, but the small size limited fiber diameters to eight microns, and would not work for testing the eleven micron diameter Mitsubishi carbon fibers. In order to measure the thermal diffusivities of a wide-ranging size of micro/nano wires a new thermal sensor needed to be developed.

A 1D implicit numerical model was developed based on the experimental configuration to help determine optimal system dimensions. The model allows input of the size and thermal characteristics of the fiber, sensor, and heat sinks. The model assumes an instantaneous temperature jump at the point of contact between the heater and fiber as well as a constant ambient temperature at the heat sink. The model then uses finite difference methods to determine the temperature rise of the sensor using a one dimensional heat conduction equation, from which a resistance change can be determined using the sensor's temperature coefficient of resistance. Once the resistance change has been found, the model uses the room temperature resistance of the system as well as the amount of current being passed over the sensor to determine the magnitude and shape of the measured voltage change. By varying the many inputs to this model, an optimal voltage curve can be found that greatly speeds up the experimental measurement process.

This model was used in order to optimize the design of the SEM stage. It is found that the use of aluminum wire used in wedge wire bonding would make a very good sensor. Its twenty-six micron diameter and excellent properties allow this sensor to be used for measuring micron sized fibers as well as wires as small as one hundred nanometers. The numerical model also helped determine the optimum length of the sensor to be around three hundred microns, more than enough length to easily place our sample fibers.

An ideal sensor must be easy to work with, have as small a width and thickness as possible, and most importantly display a high temperature coefficient of resistance. The temperature coefficient of resistance is a measure of how much a material's resistance changes with temperature, and in order to get the strongest signal possible this value must be maximized. Ultimately aluminum was chosen as the sensor material as it is very easy to work with and has a very high temperature coefficient of resistance. In order to actually construct the sensor, a thin aluminum wire and a means for constructing a circuit were needed. It was decided to use wire bonding as this is a rather simple and convenient means of making electrical connections and is commonly used for joining integrated circuits and printed circuit boards. Wire bonding uses a combination of pressure and ultrasonic energy to make a weld between a thin diameter wire and a flat surface. The wire bonder used to construct the sensor for this work uses aluminum wire approximately twenty-six microns in diameter and welds this wire between two copper pads.

After deciding to use aluminum as the sensor material, the entire stage that would be placed inside the SEM needed to be designed as shown in Figure 17.

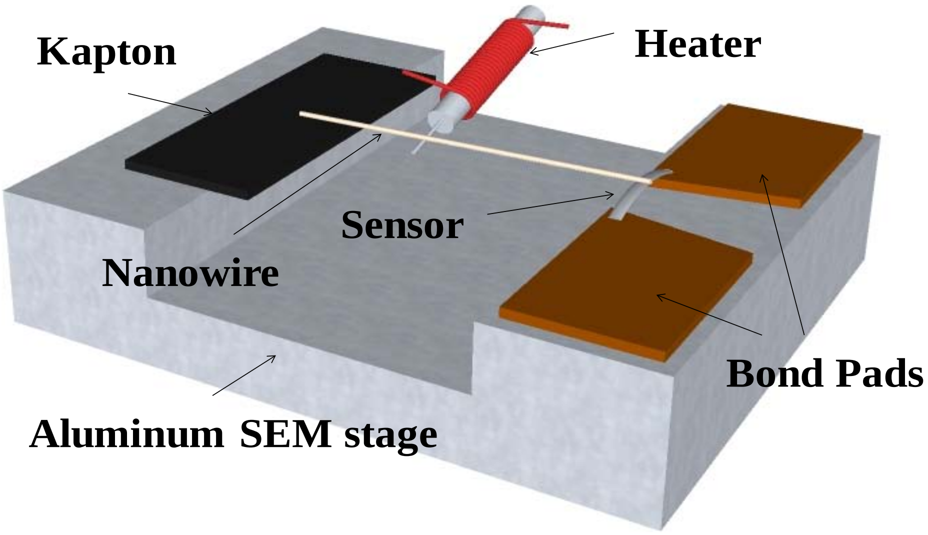

Figure 17: 3D model of the fully designed stage as it is used inside of the SEM.

For the heat sink, copper is chosen as it has a very high thermal conductivity and it is very easy to wire bond. An aluminum stage was built that comprised raised edges approximately twenty millimeters apart, over which our micro/nanowires would be suspended. On one of the raised sections, the two copper pads were positioned as close together as possible, without touching. These pads were then epoxied to the aluminum stage in order to fix them in place and to electrically insulate them from the stage. The next step was to fix wires to each of the bond pads that would be used to pass a current across the wire bond sensor. The final step was to use a wedge wire bonder to mechanically fix the small aluminum wire between the two copper pads.

3.5 Heater Design

The nichrome wire used to create the heaters was provided by California Fine Wire Company and has a diameter of approximately 0.005 inches. The heaters are built by wrapping an insulated nichrome wire around a micromanipulator probe in two overlapping layers. These layers are approximately one centimeter long, and account for a total resistance of just over thirty ohms. The heater has free range of motion inside of the SEM through the use of a Kleindiek MM3A-EM micromanipulator so that it may contact the micro/nanowire at any point along its length. The wire is held in place on the micromanipulator probe using a very small amount of high temperature epoxy. The heaters were tested under high vacuum using a small thermocouple to quantify their temperature as a function of input current with results shown in Figure 18.

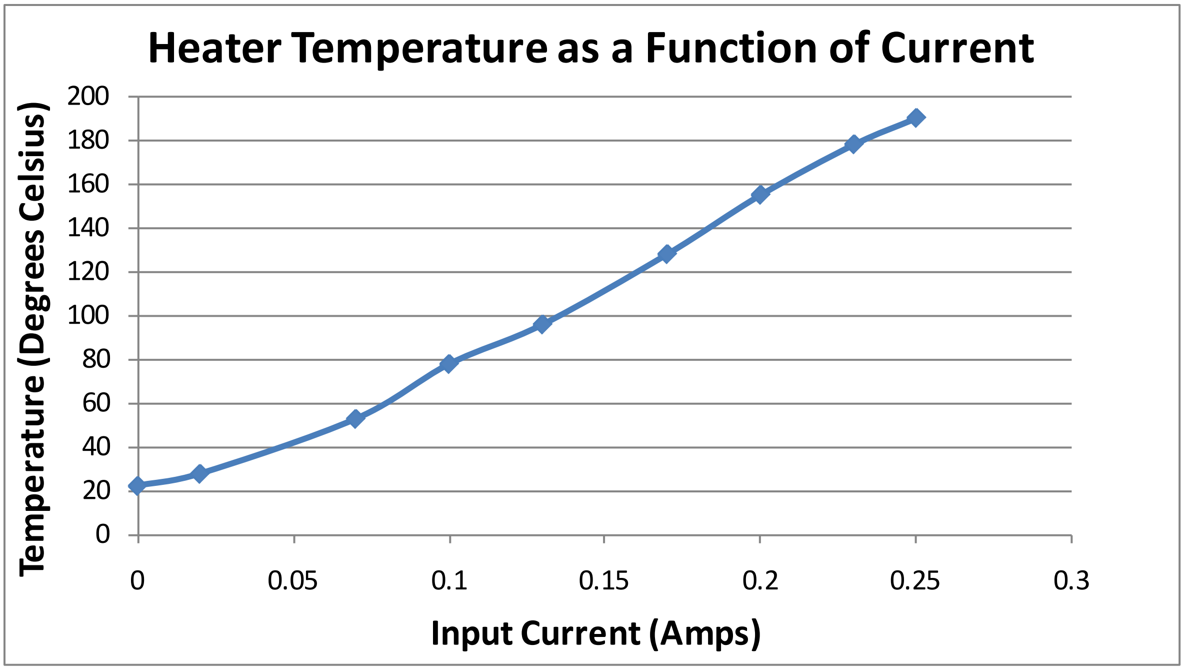

Figure 18: This graph depicts the measured temperature of the heater as a function of the input current. This was useful for modeling the experiment and in order to induce a measurable resistance change in the sensor.

For these tests the current was slowly increased from 0 to 0.25 amps while the temperature was recorded. The results from this test were useful for numerical modeling of the thermal flash method by providing the temperatures a heater would likely reach during a test.

3.6 Experimental Approach

The experimental configuration is shown above in Figure 17, and an SEM image from testing the University of Akron fibers is shown below in Figure 19. The thermal sensor is comprised of an aluminum wire bonder wire connected between two large copper heat sinks. Inside the SEM, the fiber to be tested is positioned on top of the thermal sensor on one end and a Kapton prop on the other, suspending the fiber for most of its length. The fiber is normally held in place mechanically to avoid any movement while testing. The micromanipulator is heated by passing a current through a polyimide-coated nichrome wire wrapped along its length. The manipulator is positioned an appropriated distance from the sensor, depending on the expected diffusivity of the fiber, and in close proximity to the fiber. The electron beam is then turned off and the manipulator is moved until it comes in contact with the fiber, causing an instantaneous temperature change in the fiber, initiating thermal diffusion through the length of the fiber and into the sensor. The temperature rise of the sensor causes a similar change in the resistance of the sensor, which is used to numerically calculate the diffusivity of the fiber.

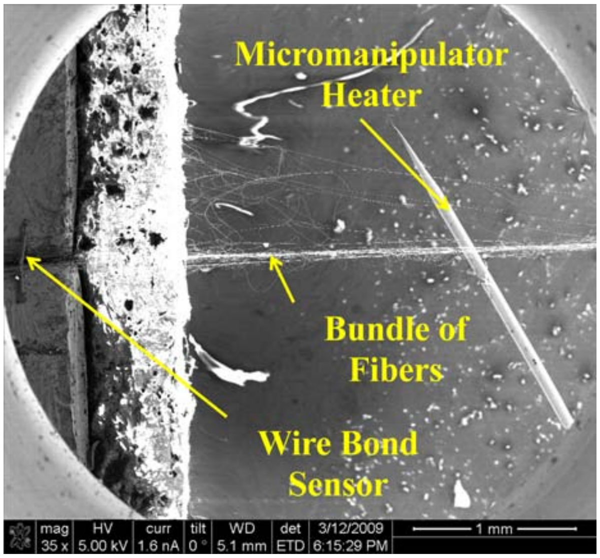

Figure 19: This SEM image shows the testing of University of Akron fibers. The heater, sensor, and fibers are all labeled to help show the one dimensional heat conduction path.

Current is pulsed over the sensor and the voltage drop is continuously measured during the experiment. As the sensor heats up due to thermal conduction through the fiber, its resistance will change, causing the voltage to change as well. This method of passing a current over a sensor and measuring voltage is hampered by the need for a small sensor in this measurement. If a continuous DC current is passed across the sensor, its temperature would continuously rise. In order to avoid this problem of self-heating, a method known as the two-point delta technique is used as depicted in Figure 20.

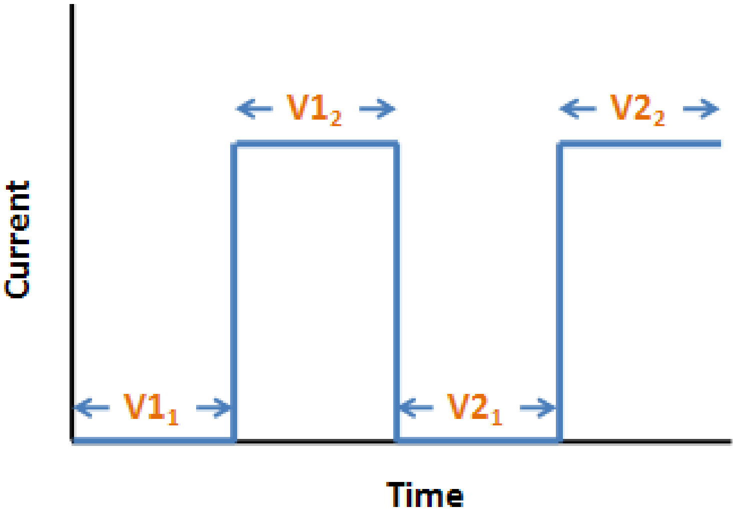

Figure 20: Delta Mode Measurement. Each voltage point is calculated by taking the difference between the measured voltage before and during the current pulse.

In the two-point delta mode measurement depicted above, current is sourced as pulses and voltage is measured before and during each pulse. The measured voltage is calculated as follows:

$$V1_2 - V1_1 = V1$$

$$V2_2 - V2_1 = V2 \tag{3.10}$$

As shown in equation 3.9, the difference between these two voltage readings is taken as the measured voltage, thus reducing any thermoelectric offsets. This technique is carried out using a Keithley 6221 current source mated with a Keithley 2182 nanovoltmeter. These instruments work together in order to measure as quickly as possible, making a measurement every 25 milliseconds.

The temperature of the sensor is not able to be directly measured due to size limitations. Instead, the voltage change is measured and used to find the temperature change. Electrical resistance is a function of temperature, therefore the shape of the temperature vs. time curve should be exactly the same shape as the voltage vs. time curve. Therefore the experimentally measured voltage change has the exact same exponential shape as the sensor's temperature rise. For this method only the shape of the curve is important and the magnitude has no relevance. The experimentally measured voltages get normalized between 0 and 1 and the analytical solution is used to fit a temperature rise to the voltage rise. Because the voltages and temperatures get normalized, thermal contact resistance will not influence the measurement as they would have no effect on the shapes of the curves, only affecting the magnitudes. Using the analytical solution in conjunction with the normalized experimental voltage data, the thermal diffusivity of the test fiber can be found. A curve fitting procedure is used to minimize the sum of the squared error between the voltage data and the analytical solution.

3.7 Thermal Flash Limitations

The thermal flash technique is a good method that reduces complexities and errors imposed by other measurement techniques, yet like all methods it has limitations. As discussed in section 2.5, the exponential rise time is a function of both the materials thermal diffusivity and the length of the fiber. If a very short fiber length is used, the exponential rise time becomes extremely short, too quick for the nanovoltmeter to read. Instead of measuring an exponential, the instrument will measure a discontinuity. Without very fast voltage readings, the discontinuity could never be represented as its true exponential form. Current instruments used in this experiment can make one measurement every 25 milliseconds, requiring exponential rise times around 0.2 to 0.3 seconds for accurate thermal diffusivity measurements. Using a fiber length shorter than what would produce these rise times leads to a loss of certainty and precision. The second limitation of this technique is that it measures thermal diffusivity and not thermal conductivity. The density and specific heat of the test sample must be known in order to properly report thermal conductivity values. There is no possible way to avoid this without using a steady-state method and introducing thermal contact resistances, but the fiber length limitation may be able to be solved with better instruments or better programming. Several of these solutions are discussed further in section 3.5.

Chapter 4 – Results and Discussion

Using the thermal flash method described in chapter 2, the thermal diffusivities of three materials have been measured. The first material tested, Mitsubishi K13D2U pitch based carbon fibers, were chosen as a test sample to verify the accuracy of the method. These melt spun fibers have a known thermal diffusivity, and are more than six centimeters long and 11 microns in diameter, so they are easy to work with. Later, Applied Sciences, Inc. (ASI) provided Pyrograf 1 vapor grown carbon fibers which were tested to demonstrate the thermal flash method's ability to measure extremely thermally conductive fibers and to attempt to provide validation of a measurement from 1985.[1] These fibers are grown in rather large mats with individual fibers about six microns in diameter which introduced some new challenges. Lastly, newly developed electrospun composite fibers produced at the University of Akron were measured. These fibers were produced specifically to create new thermal management materials and are a combination of polyimide and coal tar pitch. An experimental investigation into the relation between the fiber's thermal conductivity and their pitch content was undertaken. The results from all of these tests are further discussed below.

4.1 Mitsubishi K13D2U Carbon Fibers

Manipulation of the K13D2U fiber was done by hand because their size allows them to be seen with the human eye. The fibers come in groups and separating a long single fiber was the first challenge. After some testing it was found that pulling on both ends of a long group of fibers was usually enough to pull a few single fibers apart. Using tweezers to pick them up, they could be laid on top of the SEM stage. By viewing the sensor under a light microscope while placing the fiber, it could be positioned very precisely. An SEM image of the Mitsubishi fiber on an aluminum sensor can be seen in Figure 21.

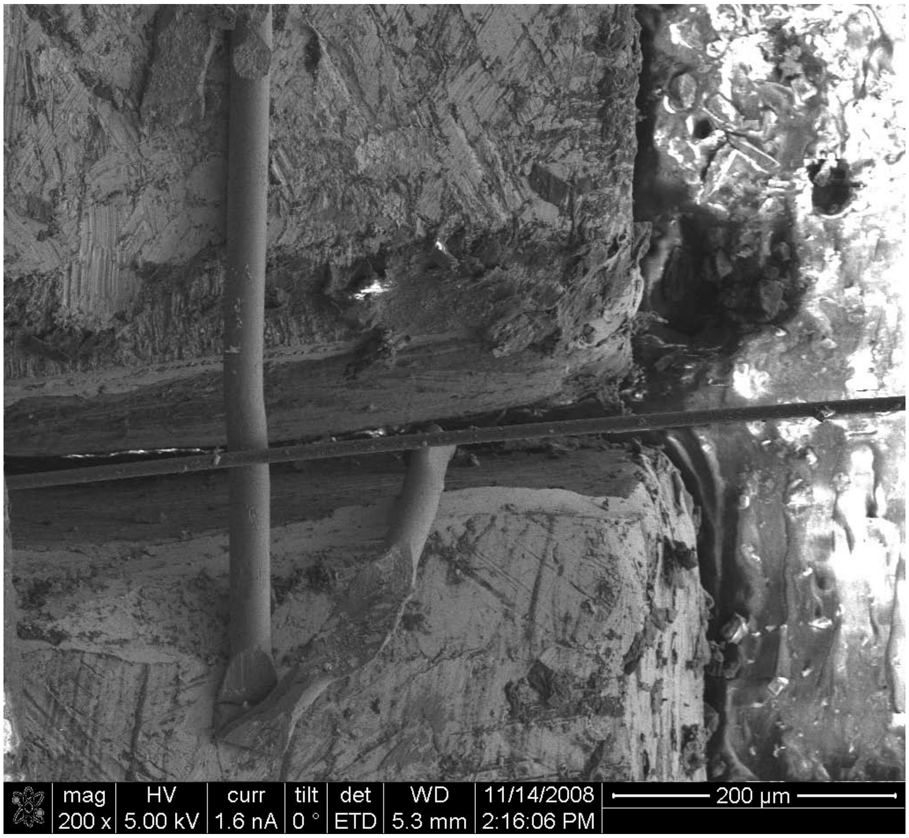

Figure 21: An SEM image showing a single Mitsubishi K13D2U carbon fiber touching an aluminum sensor. This fiber is approximately two centimeters in length.

Although the contact resistance between the fiber and the sensor will not affect the results of the test, this resistance must still be minimized in order to get a good signal. The main challenge when dealing with the Mitsubishi fibers is that they are very stiff. When the micromanipulator makes even slight contact with the fiber, it will move on the sensor, causing the heat transfer to be dispersed. When this occurs, instead of seeing a sharp change in the voltage, a more gradual change will be seen. In order to hold the fiber in place on the sensor, many methods were attempted. The first fiber tested was not held in place at all, merely rested on top of the sensor. In this test the fiber moved back and forth on the sensor not causing point heating of the sensor, hence not giving useable data. The next attempt was to use a small amount of epoxy underneath the fiber to fix it to the sensor. Unfortunately, this also did not work because the epoxy has such a low thermal conductivity that it drastically increased the thermal resistance between fiber and sensor. The third attempted solution was to use silver paste to hold it in place, since silver paste has a thermal conductivity much higher than epoxy and would cause much less of a thermal resistance. While the silver paste did reduce the thermal resistance between the fiber and sensor, it caused the heat to spread too much across the surface. It was ultimately found that by slightly bending the fiber over the sensor and holding it down with a piece of tape served best in minimizing movement and allowing the best heat transfer from fiber to sensor. While the tape holds the fiber in place, a small bead of epoxy could be applied to the fiber on both ends. This will prevent having to place tape inside of the SEM possibly leading to degassing issues.

The Mitsubishi fibers were approximately 11 microns in diameter, and the fiber lengths used for testing were between 15 and 18 millimeters. A series of 34 tests were performed on several fibers over several weeks in order to fine tune the setup and examine the accuracy and precision of the method. A sample set of data obtained from the testing of the K13D2U fibers can be seen in Figure 22.

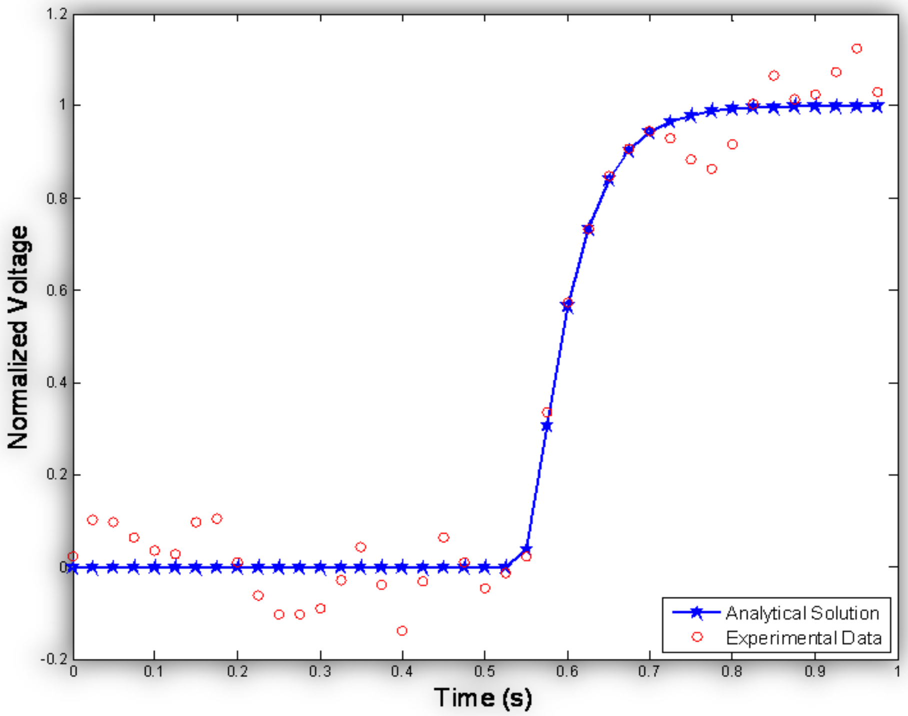

Figure 22: A sample data set showing the fit between the analytical solution of the temperature of the sensor and the experimentally measured voltages for a Mitsubishi carbon fiber about 18 millimeters in length.

The overall results from these tests as well as the other materials can be seen in Figure 23 and further summarized in Table 1. Of all fibers tested, most of the tests were performed on this fiber in order to show proper validation of the method as well as the true standard deviation of the method. The overall measured value was within 5% of the reported value,[19] showing great overall accuracy. Also, by running such a large number of tests it was determined that the true standard deviation among measurements should be around 12-15%. Further testing of fibers will not need so many measurements as it can be assumed that for similar rise times this standard deviation will not change among materials.

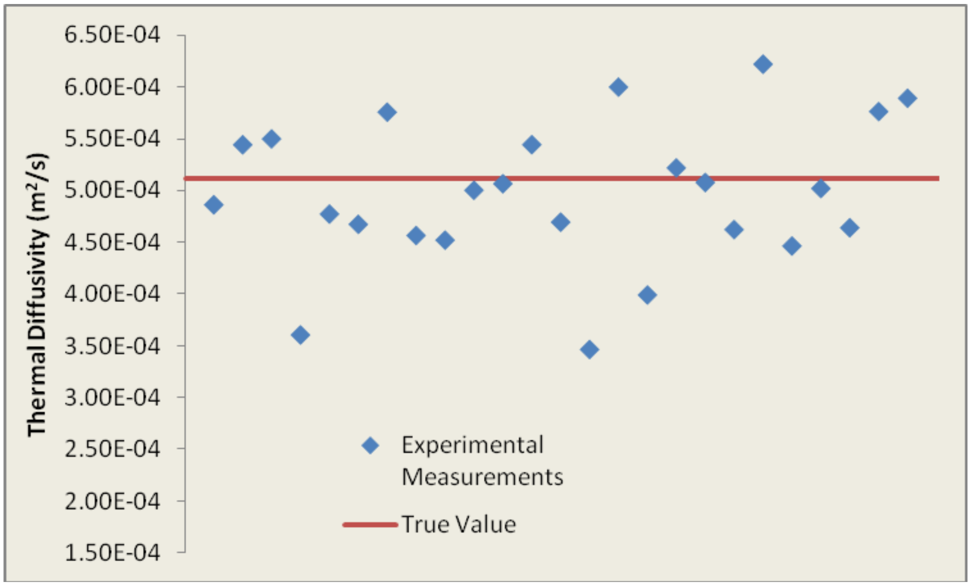

Figure 23: Summary of all measurements made of the thermal diffusivity of Mitsubishi K13D2U fibers. Computed values agree relatively well with the true value.

4.2 Applied Sciences Inc. Pyrograf I Vapor Grown Carbon Fibers

ASI Pyrograf I fibers were chosen for testing for two purposes: to validate a measurement from 1985[1] and to further the range of tested materials with the thermal flash technique. As the thermal diffusivity of the test material increases, the necessary fiber length also increases as described previously in section 3.2. Therefore, in order to test the Pyrograf I fibers, a fiber length of over 3 cm was necessary to achieve the desired exponential rise time. Testing materials with even higher thermal diffusivities than the Pyrograf I fibers will most likely need better electronics because having to use even longer fibers is not practical for testing and also generally not possible due to production limitations. Preliminary tests of the Pyrograf I fibers were performed on the short staff fibers with shorter than desired lengths due to a lack of availability of longer fibers. These tests showed fairly good accuracy with the known value, although due to a very fast exponential rise time as depicted in Figure 24, good precision was not possible. By using longer fibers the rise time will increase, allowing better measurement accuracy. The results from these preliminary tests prove that the thermal flash method is capable of measuring a very wide range of materials, including those that are even more thermally conductive than what have been measured here.

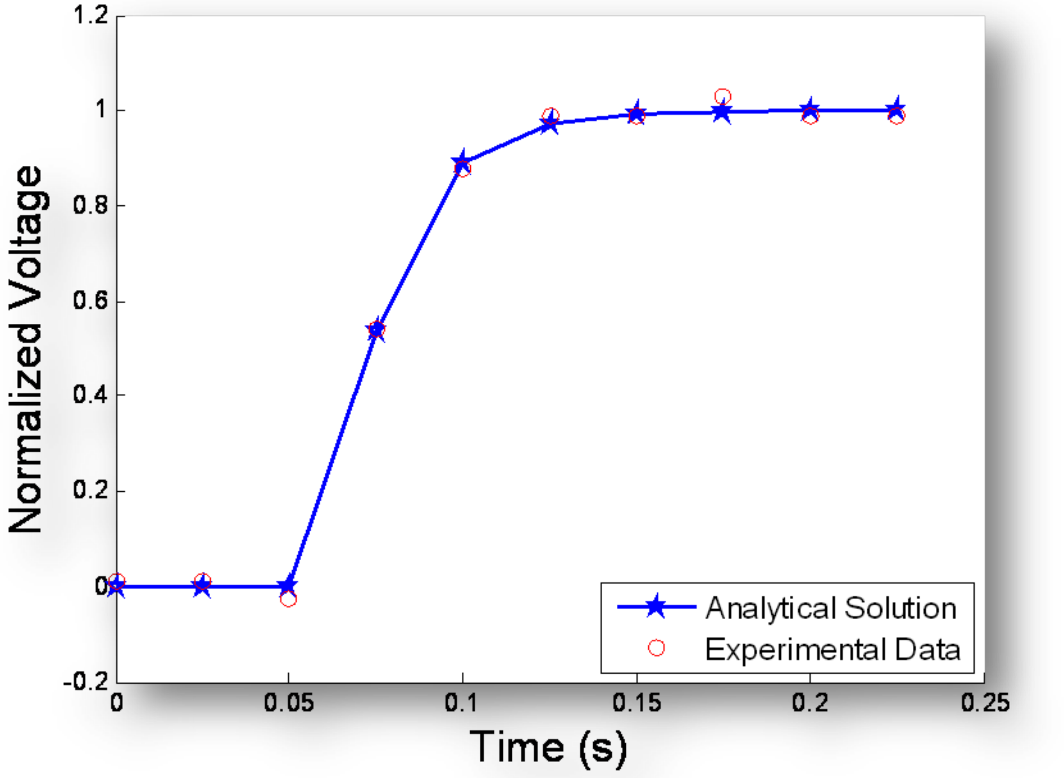

Figure 24: A sample curve fit between the analytical solution of the temperature of the sensor and the experimentally measured voltages for an ASI Pyrograf I single fiber about 17 millimeters in length. The rise time can be represented with only four data points causing a high standard deviation among measurements.

The only other Pyrograf I fibers available are those grown in forests as described in section 2.2. Individiual fibers with long lengths were not able to be isolated and thus a small bundle of approximately twelve fibers all running in one direction were used for testing. This bundle was almost four centimeters in length and the fibers touched and were partially fused many times along this length.

When testing a single fiber in the pre-described method almost all the heat entering the fiber is conducted through the sensor and into the heat sink. When testing multiple fibers that do not touch one another but all lay between the heater and the sensor, the same thing occurs, just through multiple paths. However, when these fibers touch an alternate heat conduction path opens up allowing the heat to diffuse between fibers. When testing fibers of relatively large diameters (>100 nanometers), nanoscale effects can be neglected and the resistance of heat movement from fiber to fiber is enormous compared to the resistance of heat moving directly through the fiber and into the sensor. For this reason it can be assumed that as long as the fibers run the entire length from heater to sensor, with all fibers touching at both ends, the measured thermal diffusivity for a group of fibers will return the same value as that of a single fiber. An SEM image of a group of ASI carbon fibers lying across a sensor is shown in Figure 25. As an added measure of confidence, a bundle of Mitsubishi K13D2U fibers was tested and compared to the measured values for single fibers, with statistically similar results.

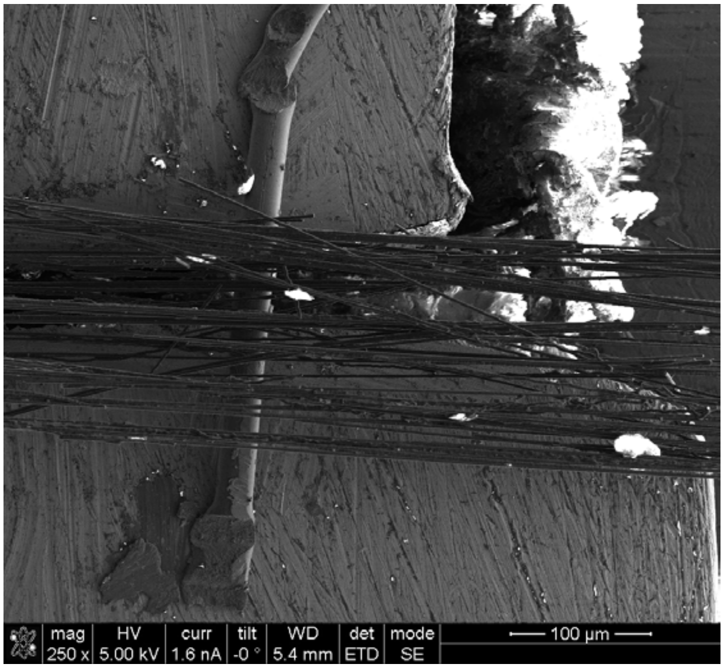

Figure 25: SEM image of the bundle of ASI Pyrograf I fibers aligned across an aluminum sensor. The fibers are relatively well aligned perpendicular to the sensor and are almost three centimeters in length.

Testing of the group of ASI Pyrograf I fibers proceeded in the same manner as testing of the single fibers. The group was cut from a large mat of fibers and was approximately three centimeters long. The mat was placed on a large SEM stage extending between the aluminum sensor and the kapton prop. Using this group of fibers a thermal diffusivity was measured that was similar to that of the single fibers, and by using a longer length, the deviation between measurements was much smaller. A summary of the measured values for the single fiber and the bundle are shown in Figure 26 and summarized further in Table 1.

Figure 26: Summary of thermal diffusivity measurements of the ASI VGCFs. The tests on the short fiber and the bundle of fibers both agree relatively well with the reported value, however the standard deviation for the bundle of fibers is much lower.

4.3 University of Akron Composite Polyimide/Coal Tar Pitch Electrospun Fibers

After validating the method using both Mitsubishi and ASI fibers, testing of an unknown material was the next goal. Focusing on thermally conductive fibers that would be good for use in thermal management composites, a new study was conducted on electrospun composite fibers from the University of Akron. These composite fibers are composed of polyimide and coal tar pitch and are between 100 and 400 nanometers in diameter with an unknown thermal diffusivity.

Working with Professor Cakmak from Akron University and his student Han Yan, electrospun polyimide fibers with the addition of coal tar pitch were obtained. These same polyimide fibers without the addition of coal tar pitch have already been tested by a previous student in the nanoEngineering laboratory at CWRU using the thermal flash method for low diffusivity materials. The addition of pitch is believed to greatly improve the fiber’s thermal conductivity but the actual thermal conductivity was unknown.

Moving the fibers from the aluminum foil onto the sensor for measurement is a rather tedious process. The individual fibers are too small to see with the naked eye and placing the entire structure under a light microscope is difficult and cumbersome. The electrospinning process also does not produce completely isolated fibers and most of the fibers overlap and are intertwined with one another. After many trial and errors of deposition and manipulation methods, the most successful technique for separating and depositing the fibers has been through the use of a height adjustable platform with two protruding parallel bars, shown in Figure 27. The bars reach in-between the ridges in the foil and underneath the fibers, and then as the platform is lifted, the fibers stick to the bars and break free of the foil. With the fibers attached to the bars and the platform, it is much simpler to freely move them. While looking at the SEM stage under a light microscope, the platform and parallel bars can be positioned such that the fibers are directly over top of the sensor. The platform is then lowered until the fibers are touching the SEM stage, and overlapping the sensor. By using a small piece of tape, the fibers can be held in place while epoxy is applied to hold them during testing.

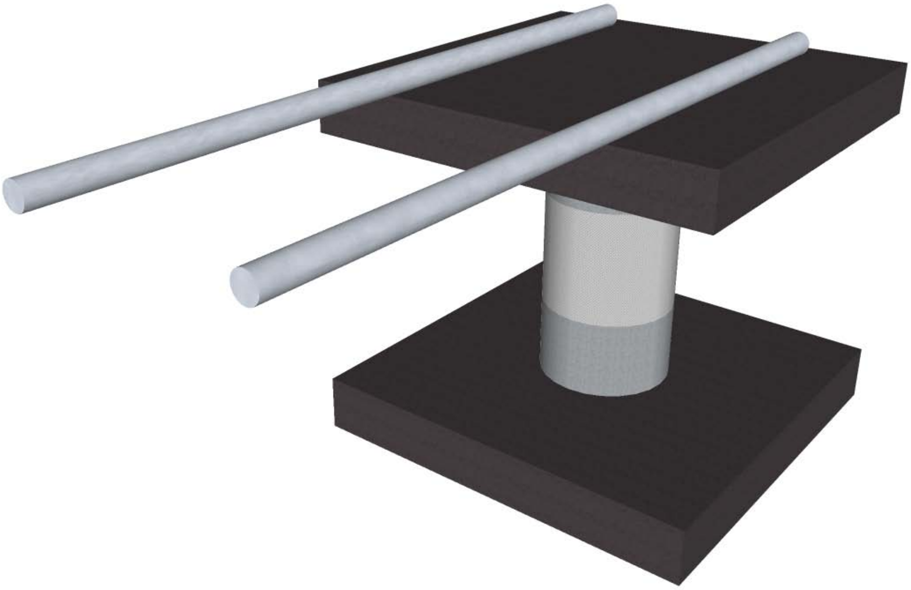

Figure 27: An apparatus designed for picking up composite fibers from the saw tooth foil and depositing them on an SEM stage. The two parallel bars are spaced to fit between the peaks in the foil but are further apart than the sensor and kapton prop.

Although techniques were developed for depositing the fibers and placing them on the stage, it was still not possible to obtain a single isolated fiber on the testing stage. Attempts to take groups of fibers and use the ion beam as well as the micromanipulator to remove excess fibers were very time consuming and not reliable. Testing of a single isolated fiber may be possible with enough trial and error, but through the previous investigation with Pyrograf I fibers, testing of groups of fibers can still produce thermal information of a single fiber. Two separate groups of fibers containing just over 9% coal tar pitch by weight have been tested, that both produced very similar results. An SEM image of one of these groups of fibers on the aluminum sensor can be seen in Figure 28.

Combining the data from these two tests led to a reported value of 71 W/m K for the polyimide fiber with 9.6% coal tar pitch.

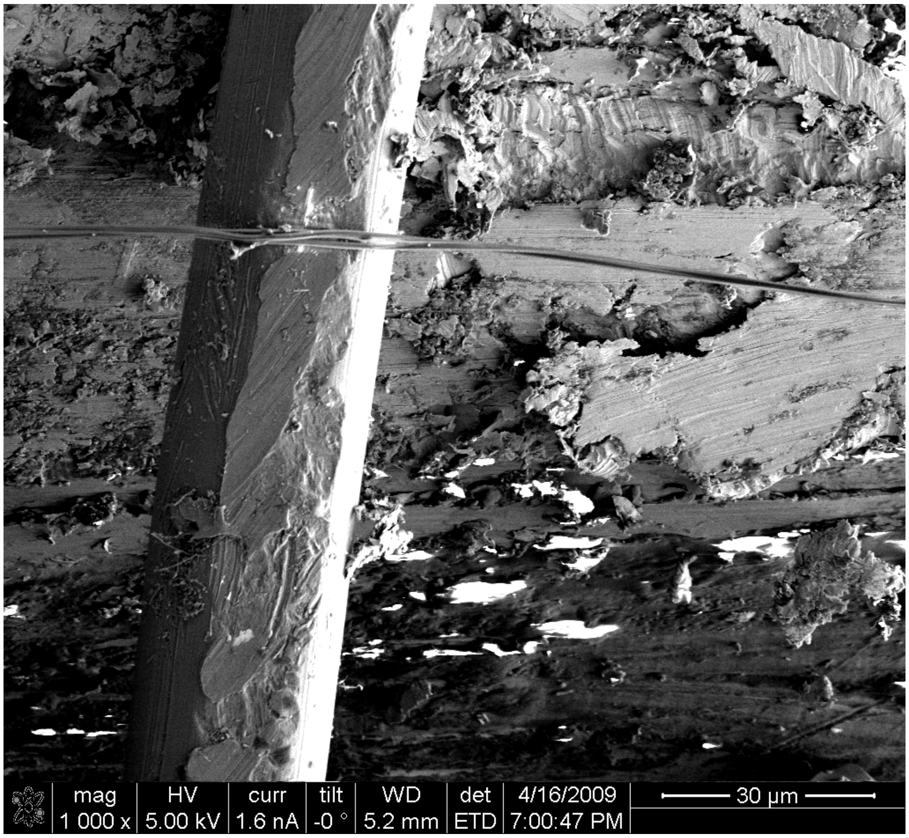

Figure 28: An SEM image of a small bundle of polyimide/pitch fibers on an aluminum sensor. The fibers are approximately 250 nanometers in diameter and are held in place using platinum deposition.

After obtaining the data on the initial batch of composite fibers, more fibers were electrospun with higher pitch contents. Testing of these fibers proceeded in a very similar manner to the first batch. All the groups of fibers tested contained a small number of fibers, generally five or less, which ran from the sensor to the kapton prop. The groups of fibers were generally held in place on the sensor using platinum deposition. These fibers were small and flexible compared to the pure carbon fibers tested earlier, so the platinum deposition worked well to hold them in place and provided good thermal contact. The summary of the measured thermal conductivities as a function of the pitch weight content is shown in Figure 29. The measurement of Demko and Abramson on a single pure polyimide fiber is included as a base reference point.[36]

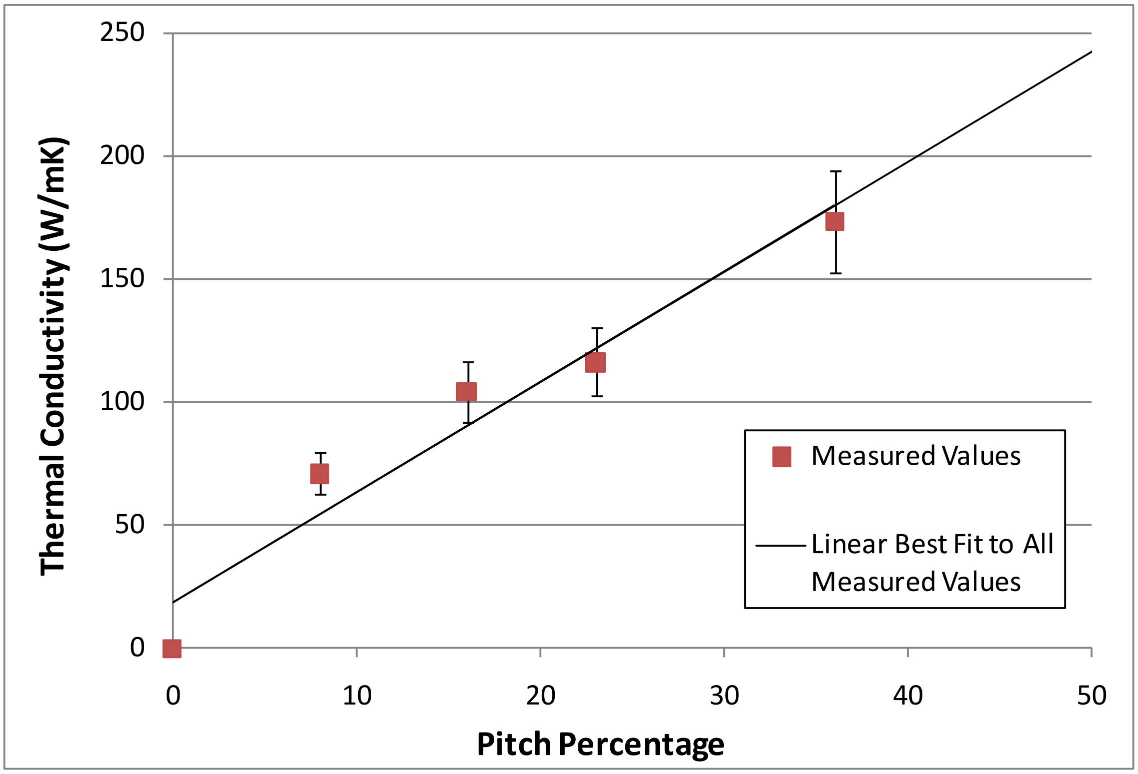

Figure 29: Thermal Conductivity vs. Pitch Percentage of the composite polyimide/pitch fibers.

As expected, the thermal conductivities follow a linear trend with percentage of pitch as predicted by an engineering rule of mixtures calculation. The rule of mixtures is a well-known engineering tool used to predict the properties of composite materials. The rule states that a physical property of a composite can be determined from a volume weighted average of the properties of the composites constituents.[33,34] Applying the rule to find the thermal conductivity of a composite made up of phases A, with thermal conductivity k_A and volume fraction V_A, and B, with thermal conductivity k_B and volume fraction V_B, would appear as follows:

$$k_{Composite} = V_A k_A + V_B k_B \tag{4.1}$$

The rule of mixtures is applicable for use with the University of Akron fibers because by dissolving pitch in the solvent it is evenly dispersed in the polyimide matrix. The upper value of thermal conductivity cannot be known exactly because pitch is relatively insoluble and thus a 100% pitch fiber cannot be solution spun. In fact, the 36% pitch content fiber is the most pitch that was able to be dissolved and still be electrospun. As mentioned in section 1.5, the thermal conductivity of pitch derived fibers varies widely depending on production methods and heat treatment conditions. Therefore it is not possible to determine what the thermal conductivity of a fully pitch fiber would be if it was able to be electrospun. The linear curve can be extrapolated to 100% pitch content resulting in a thermal conductivity of 466 W/m K, which falls within the range of measured values for pitch based carbon fibers. This value is actually quite high considering that the fibers were only heat treated to around 400° Celsius rather than to graphitization temperatures which range between 2400° C and 3000° C. If these fibers were heated to such extremes, it is likely that they would also exhibit extremely high thermal conductivities. For now it is not possible to test such fibers because more research must be conducted in order to determine how to prevent the fibers from falling apart during such processing.

It is also interesting to see that the linear fit to the data does not exactly match some of the lower values. A similar trend was found by Chen et al. who was testing the thermal conductivity of epoxy composites with the addition of the ASI Pyrograf I fibers.[35] Chen's data exhibited a linear relation between fiber content and thermal conductivity, although when extrapolated to zero fiber content, the curve does not match the thermal conductivity of epoxy. Chen did not bother trying to explain this inconsistency, so a simple explanation may not be possible.

An explanation for why the data presented here does not exactly match a linear line is likely a result of fiber production. The pitch content of a single fiber is almost impossible to compute directly, so based on the composed solution the content of the fiber can be assumed. However, as the fiber forms on a substrate, the solvent used to dissolve the polymer and pitch evaporates. This evaporation is accounted for when computing pitch content yet there still could be some inaccuracy in this measurement. Also, it is assumed that the solvent perfectly dissolves the pitch and polyimide and into an isotropic mixture. However, this is not exactly the case, and often the pitch does not fully dissolve due to its high insolubility.

When the fibers are spun they actually contain less pitch than is believed due to some pitch never fully integrating with the polyimide. This theory would be especially true for the higher pitch content fibers because the solution can only handle a certain amount of pitch but beyond this value it is no longer dissolved. These lower pitch contents would cause reported values to be lower than predicted by the rule of mixtures. This explanation can be backed up with high magnification optical images showing that some of the high pitch content fibers were not isotropic, and regions can be seen where pitch is not fully dissolved. Figure 30 shows two optical images, one of a fiber with significant pitch content displaying regions of non-dissolved pitch and a second showing a low pitch content fiber exhibiting excellent uniformity.

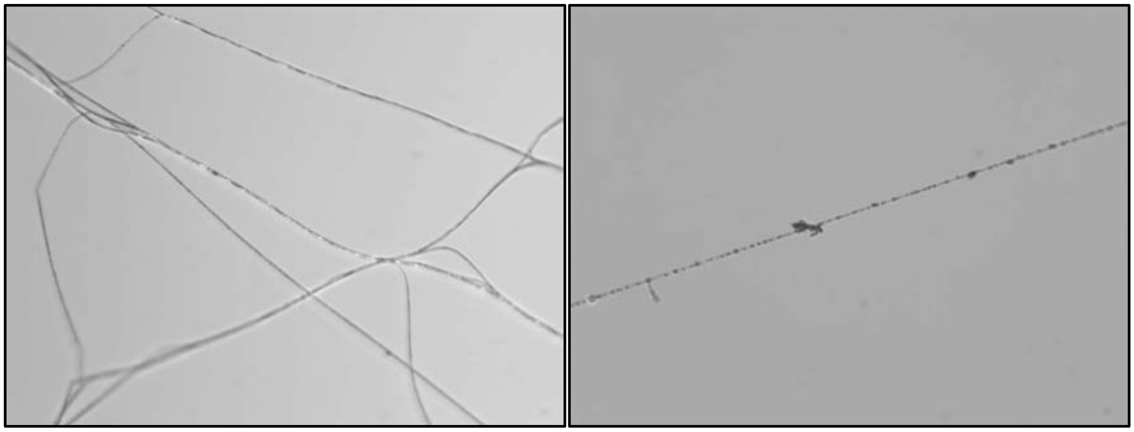

Figure 30: These optical images show polyimide/coal tar pitch fibers with two different percentages of pitch. Those on the left contain 9.6% pitch and show little to no undissolved carbon along the length of the fibers. The fibers on the left are 36% pitch fibers and it can be seen that not all the carbon is fully dissolved in the fiber. This could explain why the measured thermal conductivities for the 23% and 36% fibers are lower than expected.

If it can thus be assumed that the two upper thermal conductivity values are incorrect due to an overestimation of pitch content, a new curve may be plotted displaying the actual thermal conductivity vs. pitch content.

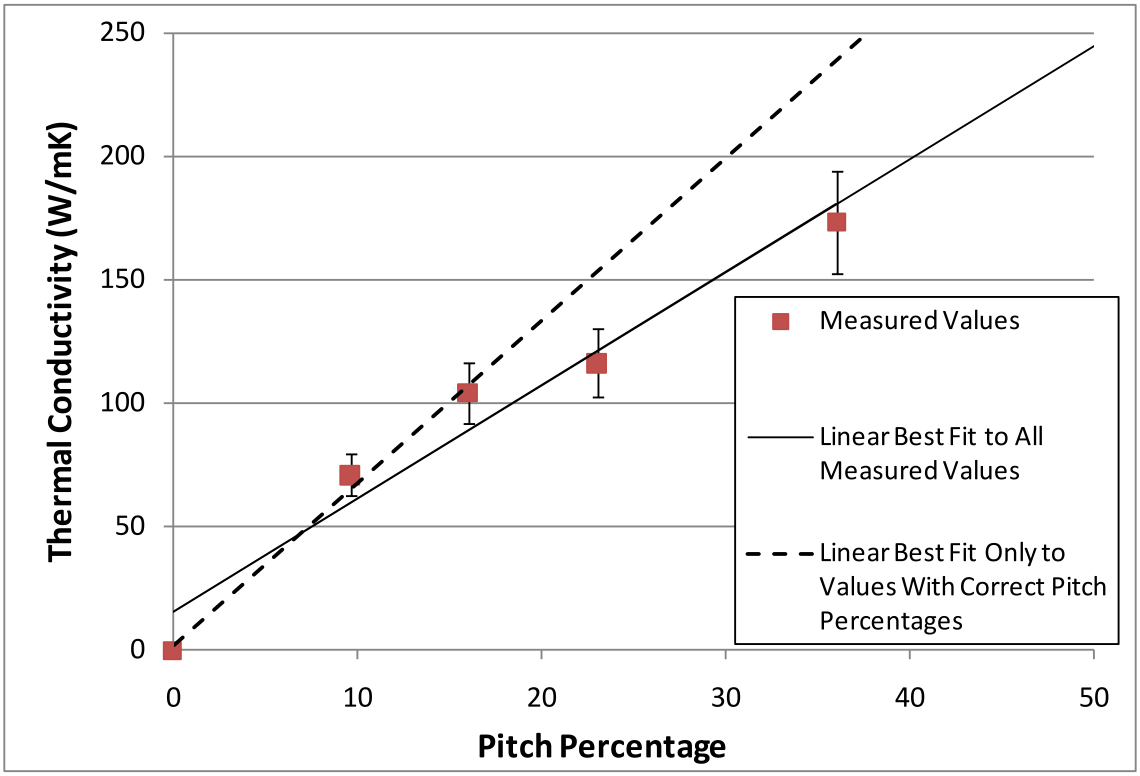

Figure 31: This is the updated fit between pitch percentage and thermal conductivity for the composite fibers. This curve is plotted only through the first 3 points because the 23% and 36% pitch percentages are too high and not accurate.

In this graph, the blue dashed line is the updated thermal conductivity of the fibers as a function of their pitch content. When extrapolated to 100% pitch content, this trend gives a thermal conductivity of 661 W/m K which is still within the range of measured values for mesophase pitch carbon fibers. This value is most likely more correct as it accounts for errors due to pitch not fully dissolving within the high pitch content fibers.

Although the measured thermal conductivities of the electrospun composite fibers are not extremely high, these fibers were only heat treated to around 400° Celsius. Most fibers tested in literature were all graphitized at extremely high temperatures between 2400° C and 3000° C. The lack of post-processing needed to produce thermally conductive polymeric fibers is the real draw here, combined with the ability to create well aligned flexible composites from these thermally conductive fibers.

4.4 Conclusions

This work introduces the thermal flash method for measuring the thermal properties of high thermal diffusivity micro and nanoscale fibers. This technique eliminates error caused by thermal contact resistances and allows for accurate and rapid testing of electrically conductive and insulating materials. Compared to other current techniques the limitations of this method are far lower and the accuracy is very similar. The results from all materials tested are provided in Table 1.

Material	Number of Measurements	Measured Thermal Diffusivity (m^2/s)	Standard Deviation (m^2/s)	True Thermal Diffusivity (m^2/s)	Percent Error
Mitsubishi K13D2U Carbon Fibers – Single Fiber	31	$4.91\cdot10^{-4}$	$0.76\cdot10^{-4}$	$5.12\cdot10^{-4}$	4.1%
Mitsubishi K13D2U Carbon Fibers – Bundle	10	$5.1427\cdot10^{-4}$	$0.75\cdot10^{-4}$	$5.12\cdot10^{-4}$	0.04%
Pyrograf 1 VGCFs - Bundle	6	$1.2644\cdot10^{-3}$	$0.10\cdot10^{-3}$	$1.31\cdot10^{-3}$ *	3.33% *
Pyrograf 1 VGCFs – Short Fiber	10	$1.3414\cdot10^{-3}$	$0.31\cdot10^{-3}$	$1.31\cdot10^{-3}$ *	2.55% *
Akron U 9.6% Pitch Fibers	21	$4.30\cdot10^{-5}$	$0.64\cdot10^{-5}$	Unknown	N/A
Akron U 16% Pitch Fibers	8	$6.22\cdot10^{-5}$	$0.49\cdot10^{-5}$	Unknown	N/A
Akron U 23% Pitch Fibers	5	$6.91\cdot10^{-5}$	$0.85\cdot10^{-5}$	Unknown	N/A
Akron U 36% Pitch Fibers	8	$1.02\cdot10^{-4}$	$0.16\cdot10^{-4}$	Unknown	N/A

* - Indicates a measurement from 1985 with its own error and is not necessarily an exact value.[1]

Table 1: Summary of all measurements conducted with the thermal flash method for this study.

This method was first tested and validated using Mitsubishi K13D2U carbon fibers because these fibers have known thermal properties and are easy to manipulate and thus easy to test. The next material tested was ASI’s Pyrograf I vapor-grown carbon fibers. These fibers present a new challenge because the length of separated individual fibers is lower than desired for precise testing. As a result, the fibers need to be tested in long narrow bundles. At first it was not known whether the values measured for single fibers could be compared to those from a bundle, so bundles of Mitsubishi fibers were tested and compared to measurements on a single fiber. The results show conclusively that testing of bundles and single fibers give the same results provided that the fibers run the complete test length and have large enough diameters as not to introduce nanoscale effects such as phonon confinement.

After the initial testing of carbon fibers with known thermal properties a new study was undertaken on electrospun composite fibers from the University of Akron. These fibers are composed mostly of polyimide with varying concentrations of coal tar pitch. By altering the weight composition of pitch and polyimide it could be seen how the thermal properties of the fibers are affected by pitch concentration. For this study four different fibers were tested with pitch concentrations of 9.6%, 16%, 23%, and 36% with the results of these tests displayed in Table 1.

Analyzing the test measurements of the composite fiber show some interesting results. First, the measured thermal conductivities are quite high for a material composed mostly of a polymer. It is also seen that a perfect linear fit cannot be made to the data for thermal conductivity vs. coal tar pitch. After much analysis it is found that this is likely due to an overestimation of pitch content in the 23-36% fibers. Due to the insolubility of mesophase pitch, adding too much does not lead to a uniform fiber but causes “chunks” to form along the length of the fiber that have not fully dissolved. These chunks do not contribute as much to the thermal conductivity of the fiber as they would if they were fully dissolved and integrated along the fibers length.

By fitting a line to the data for only low pitch content fibers, a more accurate representation of the thermal conductivity of the composite fibers as a function of pitch is made. Extrapolating this line to 100% pitch content gives a thermal conductivity of 661 W/m K. Although such a fiber could not be spun, it could be achieved through carbonization of the fiber. This value matches quite well to what other authors have reported measuring for fully mesophase pitch based fibers, although their fibers typically must be heated to much higher graphitization temperatures to display such thermal conductivities. These new composite fibers may provide a means to produce relatively high thermal conductivity fibers with much lower heat treatment.

4.5 Future Work

The work from this thesis shows a fast and easy method for accurately and reliably measuring a wide range of micro and nanostructures. This method can be applied for use with almost any material but the next focus could be on measuring the composite fibers from the University of Akron after different stages of heat treatment. It will be interesting to see how the thermal conductivity changes through carbonization and ultimately how high it can go through graphitization.

Another interesting material to test is carbon nanotubes. In its present state this method cannot measure their properties due to their limited available lengths. With the current test setup, a carbon nanotube almost six centimeters in length is needed to obtain a reliable measurement. Nanotubes available today typically come with maximum lengths around 1 to 2 centimeters, too short for testing with the current setup. The necessity for a certain fiber length can never be eliminated using the thermal flash technique but it may be able to be significantly reduced through better instruments and Labview programming.

Currently, the use of the two point delta measurement technique limits the voltage measurements to one every 25 milliseconds. However, if a direct DC current is run, the nanovoltmeter can measure as fast as 5 milliseconds. Running such an experiment would introduce new problems. By making measurements far below the power line cycle frequency, sixty hertz noise is introduced into the measurement data which needs to be filtered and removed through some exterior filters. The digital and analog filters could also be enabled on the nanovoltmeter to diminish the noise but the measurement frequency is reduced to 7 milliseconds. By using a direct DC current, self heating of the sensor is more likely to occur, possibly introducing more noise and uncertainty to the voltage data.

A second possible measurement solution is to not use a direct DC current but instead still use a pulse method but with only a single voltage measurement. Such a technique allows higher duty cycles, possibly allowing measurements faster than those used currently. Such a technique has not been attempted yet, so the actual maximum obtainable measurement speed is not known. This technique would also move the measurement frequency higher than power line cycle frequency introducing the same sixty hertz noise.

Another interesting addition to this method would be to test the thermal properties of mechanically strained fibers. The configuration of the thermal flash method would allow rather easy integration with a force transducer. By placing a Hysitron force transducer, depicted in Figure 31, on the end of the SEM stage currently containing the kapton prop, fibers would be able to be deposited between the thermal sensor and the force transducer. Before thermally testing a fiber, a strain could be placed on the fiber which could change its thermal properties.[36] The force transducer can provide a minimum z-displacement of 0.2 nanometers, allowing very fine strain control.

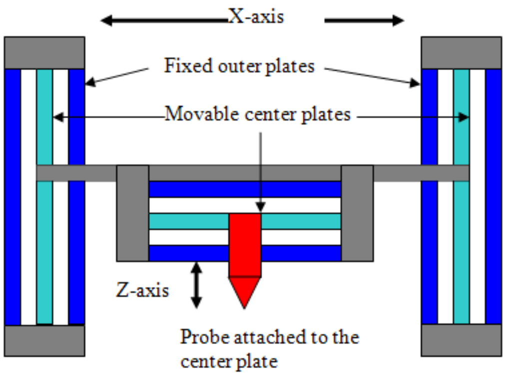

Figure 32: This is a force transducer produced by Hysitron that is capable of nanoscale displacements. This device could be easily implemented with the thermal flash method to measure thermal conductivity of mechanically strained fibers.

Appendix

A.1 Derivation of an Analytical Solution for the Sensor's Temperature as a Function of Time

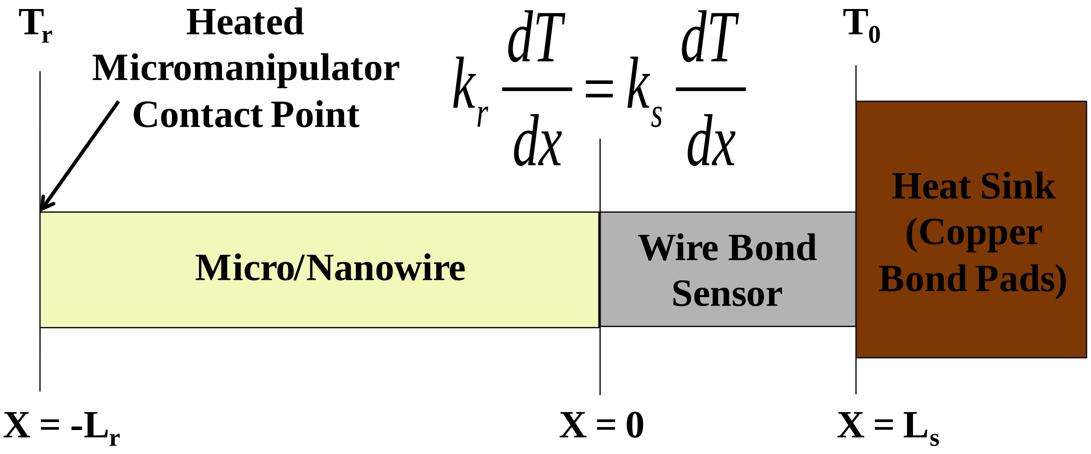

Figure 33: 1D model for thermal flash technique

Using the situation outlined in Figure 33 an analytical solution was derived. The left end of the model is the point on the micro/nanowire that is contacted by the heater. The temperature at this point, T_r, is assumed to instantly rise to that of the heater and not change during a measurement. The far end at T_0 is the contact between the aluminum wire bond sensor and the copper heat sinks. This point is assumed to stay at ambient temperatures during testing because the heat sinks are very large compared to the test sample and sensor. In the middle it is assumed that an intimate contact exists between the fiber being tested and the aluminum sensor. The temperature at this point is unknown, and needs to be solved for. It is assumed that a constant heat flux condition exists at this point; any heat leaving the end of the test fiber must flow into the sensor.

The heat equations for this one dimensional configuration are:

$$\begin{aligned} &\frac{\partial^2 T}{\partial x^2} - \frac{1}{\alpha_w}\frac{\partial T}{\partial t} = 0 \qquad && -l_w \le x \le 0 \\ &\frac{\partial^2 T}{\partial x^2} - \frac{1}{\alpha_s}\frac{\partial T}{\partial t} = 0 \qquad && 0 \le x \le l_s \end{aligned} \tag{A.1}$$

With notation as follows:

T = Temperature	x = Position along fiber
Subscript s = sensor	Subscript w = wire being tested
t = time	l = Length
k = Thermal Conductivity	k_w = Sensor Thermal Conductivity
T_0 = Ambient Temperature	$v = T - T_0$
$\alpha = \sqrt{\frac{\alpha_w}{\alpha_s}}$	$\sigma = \frac{k_s}{k_w}\alpha$
$\bar{v}$ = Laplace Temperature Difference	λ = Laplace Coordinate
$q_w = \sqrt{\frac{\lambda}{\alpha_w}}$	$q_s = \sqrt{\frac{\lambda}{\alpha_s}}$
$V_w = T_w - T_0$	c_i = Poles of the Integrand

The boundary conditions are:

$$\begin{array}{ll} T = T_w & x = -l_w \\ T|_{x\to 0^-} = T|_{x\to 0^+} & x = 0 \\ k_w \dfrac{\partial T}{\partial x} = k_s \dfrac{\partial T}{\partial x} & x = 0 \\ T = T_0 & x = l_s \end{array} \qquad \text{(A.2)}$$

The initial condition for this configuration is:

$$T = T_0 \qquad t \le 0 \qquad \text{(A.3)}$$

In order to solve equations A.1 a new temperature must be defined as T-T$_0$ that will be notated as v. This problem is best solved in the Laplace domain so a Laplace transform is first used resulting in:

$$\begin{array}{ll} \dfrac{d^2\bar{v}_w}{dx^2} - q_w^2\bar{v}_w = 0 & -l_w \le x \le 0 \\ \dfrac{d^2\bar{v}_s}{dx^2} - q_s^2\bar{v}_s = 0 & 0 \le x \le l_s \end{array} \qquad \text{(A.4)}$$

The boundary conditions for this equation become:

$$\begin{array}{ll} \bar{v}_w = \dfrac{V_w}{\lambda} & x = -l_w \\ \bar{v}_w = \bar{v}_s & x = 0 \\ k_w \dfrac{d\bar{v}_w}{dx} = k_s \dfrac{d\bar{v}_s}{dx} & x = 0 \\ & x = l_s \end{array} \qquad \text{(A.5)}$$

$$\bar{v}_s = 0$$

The solution of the above ordinary differential equation is:

$$\begin{aligned} \bar{v}_w &= Ae^{q_w x} + Be^{-q_w x} && -l_w \leq x \leq 0 \\ \bar{v}_s &= Ce^{q_s x} + De^{-q_s x} && 0 \leq x \leq l_s \end{aligned} \tag{A.6}$$

By using the boundary conditions listed above the four variables A, B, C, and D may be found. Solving for the constants and simplifying results in:

$$\begin{aligned} \bar{v}_w &= \frac{V_w\{\cosh q_w x \sinh q_s l_s - \sigma \sinh q_w x \cosh q_s l_s\}}{\lambda\{\cosh q_w l_w \sinh q_s l_s + \sigma \sinh q_w l_w \cosh q_s l_s\}} \\ \bar{v}_s &= \frac{V_w \sinh q_s(l_s - x)}{\lambda\{\cosh q_w l_w \sinh q_s l_s + \sigma \sinh q_w l_w \cosh q_s l_s\}} \end{aligned} \tag{A.7}$$

Now the inverse Laplace transform must be taken to solve for v_s and finally T_s. The temperature of the wire as a function of time is not necessary so there is no need to solve for that as well. The inversion theorem needed to solve the Laplace transform is:

$$v_s(t) = \frac{1}{2\pi i}\int_{\gamma-i\infty}^{\gamma+i\infty} e^{\lambda t}\, \bar{v}_s(\lambda) \cdot d\lambda \tag{A.8}$$

Here γ should be chosen to be so large that all the poles of $\bar{v}_s(\lambda)$ lie to the left of the line $(\gamma - i\infty, \gamma + i\infty)$ in the complex plane. To solve this line integral, Cauchy's theorem will be applied to the boundary composed of the line that is being solved for and a circle with radius R connecting the two endpoints of the line of interest as depicted in Figure 34. In order to find the value of the line, the entire boundary will be computed and the circle portion will then be subtracted.

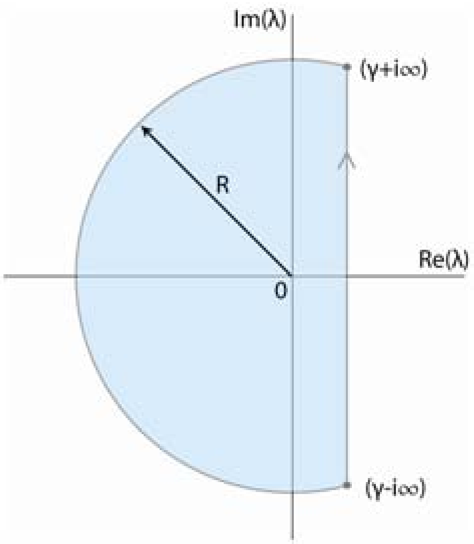

Figure 34: Evaluating the line integral using the inversion theorem. The line integral is found by using Cauchy's formula to find the line integral around the entire path and then subtracting the line integral around the portion with radius R.[37]

The line integral composing the full boundary is given by Cauchy's theorem as:

$$\oint e^{\lambda t}\bar{v}_s(\lambda)\cdot d\lambda = 2\pi i\sum_i Res\left(e^{\lambda t}\bar{v}_s(\lambda), c_i\right) \tag{A.9}$$

The function $Res\left(e^{\lambda t}\bar{v}_s(\lambda), c_i\right)$ is the residue of the function at the indicated pole. As the radius of the circle approaches infinity the value of the line integral around the circular portion of the boundary can be shown to disappear. Thus, the line integral in the inversion theorem can be evaluated to find the function $v_s(t)$:

$$v_s(t) = \sum_i Res\left(e^{\lambda t}\bar{v}_s(\lambda), c_i\right) \tag{A.10}$$

To find the value of the sum of the residues at the poles, the location of the poles of the integrand must be known. The poles are the locations that make the denominator of the function zero, and are given by:

$$\lambda\{\cosh q_w l_w \sinh q_s l_s + \sigma \sinh q_w l_w \cosh q_s l_s\} = 0 \tag{A.11}$$

It is obvious that the value $\lambda = 0$ is a pole, and by setting the expression in brackets equal to zero the others may be found. To simplify the procedure of locating the poles, we define:

$$\beta = i q_w \tag{A.12}$$

So at the poles:

$$\begin{gathered} q_w = -i\beta \\ q_s = -i\alpha\beta \end{gathered} \tag{A.13}$$

Adding these into equation A.11 leads to:

$$\cos \beta l_w \sin \alpha\beta l_s + \sigma \sin \beta l_w \cos \alpha\beta l_s = 0 \tag{A.14}$$

By solving this transcendental equation β may be found at the poles.

$$\begin{gathered} \lambda = 0 \\ \lambda = -\alpha_w \beta^2 \end{gathered} \tag{A.15}$$

The residue at a simple pole of a holomorphic function $F(z) = G(z)/H(z)$ is given by:

$$Res\{F(z),c\} = \frac{G(c)}{H'(c)} \tag{A.16}$$

Using this procedure, the residue at the poles $\lambda = 0$ and $\lambda = -\alpha_w \beta^2$ are:

$$Res\left\{\frac{V_w \sinh q_s(l_s - x)\ e^{\lambda t}}{\lambda\{\cosh q_w l_w \sinh q_s l_s + \sigma \sinh q_w l_w \cosh q_s l_s\}}, 0\right\} = \frac{V_w k_w (l_s - x)}{k_w l_s + k_s l_w} \tag{A.17}$$

$$Res\left\{\frac{V_w \sinh q_s(l_s - x)\ e^{\lambda t}}{\lambda\{\cosh q_w l_w \sinh q_s l_s + \sigma \sinh q_w l_w \cosh q_s l_s\}}, -\alpha_w \beta^2\right\} = \frac{-2V_w \sin \beta\alpha(l_s - x)\, e^{-\alpha_w \beta^2 t}}{\beta\{(l_w + \sigma\alpha l_s) \sin \beta l_w \sin \alpha\beta l_s - (\alpha l_s + \sigma l_w) \cos \beta l_w \cos \alpha\beta l_s\}} \tag{A.18}$$

Now the residues at the poles may be used in equation A.10 to find the temperature difference function in the time domain. Because β must be solved from the transcendental equation A.14, there must exist a sum over the possible values of β leading to:

$$v_s(t) = \frac{V_w k_w (l_s - x)}{k_w l_s + k_s l_w} - \sum_{m=1}^{\infty} \frac{2V_w \sin \beta_m \alpha(l_s - x)\, e^{-\alpha_w \beta_m^2 t}}{\beta_m\{(l_w + \sigma\alpha l_s) \sin \beta_m l_w \sin \alpha\beta_m l_s - (\alpha l_s + \sigma l_w) \cos \beta_m l_w \cos \alpha\beta_m l_s\}} \tag{A.19}$$

Finally, this may be modified to solve for the temperature of the sensor rather than the temperature difference, resulting in:[37]

$$T_s = T_0 + \frac{\Delta T\, k_w\, l_s}{k_w l_s + k_s l_w} - 2\,\Delta T \sum_{m=1}^{\infty} \frac{\sin \alpha\beta_m l_s \cdot\, e^{-\alpha_w \beta_m^2 t}}{\beta_m\{(l_w + \sigma\alpha l_s)\sin\beta_m l_w \sin\alpha l_s\beta_m - (\sigma l_w + \alpha l_s)\cos\beta_m l_w \cos\alpha l_s\beta_m\}} \tag{A.20}$$

A.2 Simplifying the Analytical Solution for High Thermal Diffusivity Fibers

The first step to simplifying the analytical equation is to find a solution for β. The transcendental equation used to solve for β is:

$$\sin\alpha\beta l_s \cos\beta l_w + \sigma\cos\alpha\beta l_s \sin\beta l_w = 0 \tag{A.21}$$

When $l_w \gg \alpha l_s$ the sinusoids containing the βl_w term will have much higher frequencies than those containing $\alpha\beta l_s$. Because we are trying to find the zeroes of this function and the first several zeroes are the most important, so the high frequency terms will dominate over this range. The small angle approximation may then be used on the terms containing $\alpha\beta l_s$ resulting in:

$$\alpha\beta l_s \cos\beta l_w + \sigma\sin\beta l_w = 0 \tag{A.22}$$

Looking at this equation it seems that a relation between $\alpha\beta l_s$ and σ should be made. Knowing that $\sigma = \frac{k_s}{k_w}\alpha$, a comparison may be established:

$$\frac{k_s}{k_w} \gg \beta l_s \tag{A.23}$$

$$\sin \beta l_w = 0 \tag{A.24}$$

Therefore,

$$\beta \approx \frac{n\pi}{l_w} \tag{A.25}$$

The assumption thus becomes:

$$\frac{k_s}{k_w} \gg \frac{l_s n\pi}{l_w} \tag{A.26}$$

Now the full analytical solution may be simplified beginning with the full equation:

$$\begin{aligned} T_s \\ = T_0 + \frac{\Delta T\, k_w\, l_s}{k_w l_s + k_s l_w} \\ - 2\,\Delta T \sum_{m=1}^{\infty} \frac{\sin \alpha\beta_m l_s \cdot\ e^{-\alpha_w \beta_m^2 t}}{\beta_m\{(l_w + \sigma\alpha l_s)\sin \beta_m l_w \cdot \sin \alpha l_s \beta_m - (\sigma l_w + \alpha l_s)\cos \beta_m l_w \cdot \cos \alpha l_s \beta_m\}} \end{aligned} \tag{A.27}$$

Now the value of β may be plugged in:

$$\begin{aligned} T_s \\ = T_0 + \frac{\Delta T\, k_w\, l_s}{k_w l_s + k_s l_w} \\ -\ \Delta T \sum_{m=1}^{\infty} \frac{2 \sin \alpha \frac{n\pi}{l_w} l_s \cdot\ e^{-\alpha_w \left(\frac{n\pi}{l_w}\right)^2 t}}{\frac{n\pi}{l_w}\left\{(l_w + \sigma\alpha l_s)\sin n\pi \cdot \sin \alpha l_s \frac{n\pi}{l_w} - (\sigma l_w + \alpha l_s)\cos n\pi \cdot \cos \alpha l_s \frac{n\pi}{l_w}\right\}} \end{aligned} \tag{A.28}$$

Because n is an integer, the quantity inside the infinite sum may be simplified to:

$$\frac{2l_w e^{\frac{-\pi^2 n^2 t\alpha_w}{l_w^2}} \sec n\pi \tan\frac{l_s n\pi\alpha}{l_w}}{n\pi(-l_s\alpha - l_w\frac{k_s}{k_w}\alpha)} \tag{A.29}$$

Now the first assumption must be used again to allow for further simplification and is defined as:

$$\frac{l_w}{l_s} \gg \alpha \tag{A.30}$$

Using this assumption, the tangent function from A.28 may be reduced with the small angle approximation:

$$\tan\frac{l_s n\pi\alpha}{l_w} \approx \frac{l_s n\pi\alpha}{l_w} \tag{A.31}$$

Using this simplification the infinite sum can be reduced to:

$$\frac{2l_s e^{\frac{-\pi^2 n^2 t\alpha_w}{l_w^2}} \sec n\pi}{-l_s - l_w\frac{k_s}{k_w}} \tag{A.32}$$

By now imposing the infinite sum on this simplified quantity,

$$\begin{aligned} &\sum_{n=0}^{\infty} \frac{2l_s e^{\frac{-\pi^2 n^2 t\alpha_w}{l_w^2}} (-T_0 + T_w) \sec n\pi}{-l_s - l_w\frac{k_s}{k_w}} \\ &\qquad = \frac{l_s(-T_0 + T_w)(2 + 2\sum_{n=1}^{\infty} -1^n e^{\frac{-(n\pi)^2 t\alpha_w}{l_w^2}})}{-l_s - l_w\frac{k_s}{k_w}} \end{aligned} \tag{A.33}$$

Putting this simplified sum back in equation A.27, the temperature of the sensor becomes:

$$T_s = T_0 + \frac{\Delta T\, k_w\, l_s}{k_w l_s + k_s l_w} - \Delta T\, \frac{l_s\left(2 + 2\sum_{n=1}^{\infty} -1^n e^{\frac{-(n\pi)^2 t \alpha_w}{l_w^2}}\right)}{-l_s - l_w \frac{k_s}{k_w}} \tag{A.34}$$

This equation looks much simpler than the initial equation but it can still be simplified further. When solving for the thermal diffusivity of the fiber, the voltage data is normalized so that the magnitude of the exponential is not important. In the above equation for the temperature of the sensor most of the terms deal with the magnitude of the temperature. Only the terms dealing with the shape of the curve are necessary so everything else is removed. This leaves a rather simple equation:

$$T_s(t) = 1 + 2\sum_{n=1}^{N} -1^n \cdot e^{\frac{-(n\pi)^2 t \alpha_w}{l_w^2}}\ ,\ t > 0 \tag{A.35}$$

Where,

$$N \ll \frac{l_w k_s}{l_s k_w \pi} \tag{A.36}$$

This value of N comes from the first assumption. Because the value n appears in that assumption, the sum can no longer be infinite and must only go to N as defined by A.36.

A.3 Error Analysis

To find the accuracy of the thermal flash method, the accuracy of the test instruments must be determined. The Keithley 2182A nanovoltmeter has an error of 1% for the speed at which measurements occur. However, the voltmeter also has built in noise of 70 nV at these levels with the filter turned off. For the measurements made for this work, the filter is left on so the actual noise levels of the machine are not known. It is assumed that the majority of the error in this measurement is due to the noise in the nanovoltmeter which will now be investigated. The error caused by the nanovoltmeter's noise is a function of how strong a signal is measured. The larger the magnitude of the exponential, the less effect noise will have. Looking at a sampling of exponentials analyzed for this work, errors caused by 70 nV noise averaged to about 15%. Because of additional filtering used for the measurement it can be assumed that the error of the setup is actually less than 15% but this will serve as a good approximation. By looking at the measurements made on Mitsubishi and ASI fibers, it can be seen that the majority of the data points fall within +/- 15% of the mean. This helps to reassure that the majority of the error from this measurement lies with the nanovoltmeter and is about 15%.

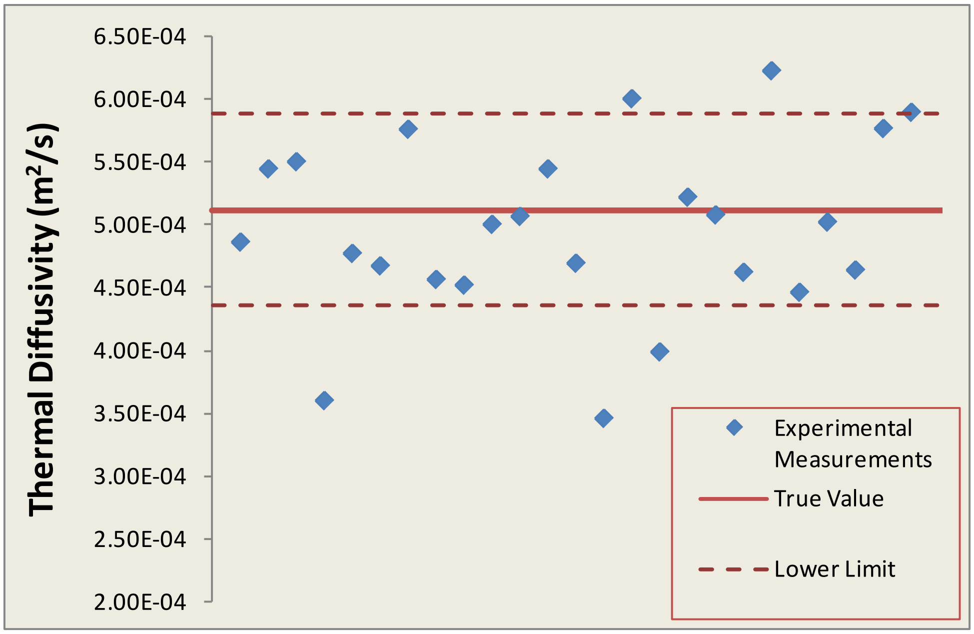

Figure 35: Summary of measurements made on Mitsubishi K13D2U fibers including error limits due to noise from the nanovoltmeter.

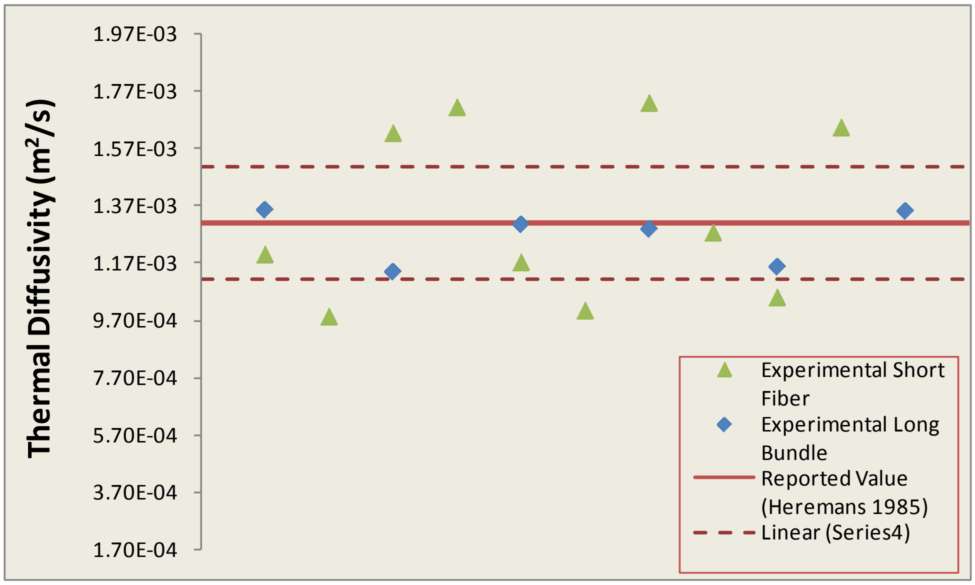

Figure 36: Summary of measurements made on ASI Pyrograf I fibers including error limits due to noise from the nanovoltmeter.

The noise that exists in the voltage data is the greatest contributor to error in this measurement. The error is not a function of the thermal flash technique, but rather due to the means of acquiring voltage data. In order to reduce variance between measurements a different voltage measuring system must be found.

When computing the standard deviation in chapter 4 it was always found as a function of the number of measurements taken. The standard deviation found is that for the given sample size and can then be related to the population. It is possible to determine the confidence in the measured thermal diffusivity by calculating the standard error of the mean as:

$$SE = \frac{s}{\sqrt{n}} \tag{A.37}$$

Here, SE is the standard error of the mean, s is the standard deviation of the sample and n is the number of measurements taken. Using statistics it is possible to create confidence intervals based on the standard error assuming normally distributed data.

67% confidence means that the true thermal diffusivity lies within +/- 1 standard error of the mean. Similarly, 95% confidence signifies that the true value lies within +/- 2 standard errors of the mean. Finally, 99% confidence indicates that the true value lies within +/- 3 standard errors of the mean. Finding the standard error for all measured data yields the following results.

Material	Number of Measurements	Measured Thermal Diffusivity (m^2/s)	Standard Deviation of the sample (m^2/s)	SE (m^2/s)
Mitsubishi K13D2U Carbon Fibers – Single Fiber	31	$4.91 \cdot 10^{-4}$	$7.6*10^{-5}$	$1.4*10^{-5}$
Mitsubishi K13D2U Carbon Fibers – Bundle	10	$5.14 \cdot 10^{-4}$	$7.5 \cdot 10^{-5}$	$2.4*10^{-5}$
Pyrograf 1 VGCFs - Bundle	6	$1.26 \cdot 10^{-3}$	$1.0 \cdot 10^{-4}$	$4.1*10^{-5}$
Pyrograf 1 VGCFs – Short Fiber	10	$1.34 \cdot 10^{-3}$	$3.1 \cdot 10^{-4}$	$9.8*10^{-5}$
Akron U 9.6% Pitch Fibers	21	$4.30 \cdot 10^{-5}$	$6.4 \cdot 10^{-4}$	$1.4*10^{-4}$
Akron U 16% Pitch Fibers	8	$6.22 \cdot 10^{-5}$	$4.9 \cdot 10^{-6}$	$1.7*10^{-6}$
Akron U 23% Pitch Fibers	5	$6.91 \cdot 10^{-5}$	$8.5 \cdot 10^{-6}$	$3.8*10^{-6}$
Akron U 36% Pitch Fibers	8	$1.02 \cdot 10^{-4}$	$1.6 \cdot 10^{-5}$	$5.7*10^{-6}$

Table 2: Summary of all measurements including standard errors.

The standard error gives a better representation of the actual thermal diffusivity of the material being tested than by use of standard deviation. Using the standard error, the true value should lay within +/- 1 standard error with 67% confidence, +/- 2 standard errors with 95% confidence, and within +/- 3 times the standard error with over 99% confidence.

References

1. Heremans J, Beetz C.P. Thermal conductivity and thermopower of vapor-grown graphite fibers. *Physical Review B* 1985;32(4):1981-1986.

2. CPU Power Densities. Intel Documents

   www.Intel.com

3. Kelly, BT. Physics of Graphite, Applied Science Publishers, London, 1981.

4. Incropera, F. P. & Dewitt, D. P. *Introduction to Heat Transfer, Fourth Edition* 2002; New York, NY: Wiley 819-831.

5. Kittel, C. Introduction to Solid State Physics, 7th edition, John Wiley & Sons, New York, 1996.

6. Berber S, Kwon Y, Tomanek D. Unusually high thermal conductivity of carbon nanotubes. *Phys. Rev. Lett.* 2000;84:4613-4616

7. Nysten B, Piraux L, Issi J-P. Thermal Conductivity of Pitch-Derived Fibers. J Phys D 1985;18:1307-1310.

8. Balandin A, Ghosh S, Bao W, et al. Superior Thermal Conducitivy of Single-Layer Graphene. *Nano Letters* 2008;8(3):902-907

9. Cahill D, Ford W, Goodson K. Nanoscale Thermal Transport. *Journal of Applied Physics* 2003;93:793

10. Biercuk, MJ, Llango MC, Radosavljevic M, Hyun JK, Johnson AT, Fischer JE. Carbon nanotubes for thermal management. *Applied Physics Letters* 2002; 80(15):1469696.

11. Donnet, J. Carbon Fibers, 3rd Edition, Marcel Dekker, New York, 1998.

12. Edie, D. The Effect of Processing on the Structure and Properties of Carbon Fibers. *Carbon* 1998;36(4):345-362

13. Piraux L, Nysten B, Haquenne A, Issi J P, Dresselhaus M S, Endo M. Solid State Communications 1984;50(8):697-700.

14. Gallego NC, Edie DD, Nysten B, Issi JP, Treleaven JW, Deshpande GV. The thermal conductivity of ribbon-shaped carbon fibers. Carbon 2000;38(7):1003-1010.

15. Mitsubishi K13D2U Data Sheet. http://www.mitsubishichemical.com/DataSheets/CarbonFiber/PD%20K13D2U.pdf

16. Reneker, D. Chun, I. Nanometre diameter fibres of polymer, produced by electrospinning. *Nanotechnology* 1996;7:216-223.

17. Chun, I., Reneker, D.H., Fong, H., Fang, X. Carbon nanofibers from polyacrylonitrile and mesophase pitch. *Journal of Advanced Materials* 1999;31(1):36-41.

18. Yang, K.S., Edie, D.D., Lim, D.Y., Kim, Y.M., Choi, Y.O. Preparation of carbon fiber web from electrostatic spinning of PMDA-ODA poly(amic acid) solution. *Carbon* 2003;41(11):2039-2046

19. May, P.W., Portman, R., Rosser, K.N. Thermal conductivity of CVD diamond fibres and diamond fibre-reinforced epoxy composites. *Diamond Relat.Mater* 2005;14(3-7):598–603.

20. Kim, P., Shi, L., Majumdar, A., McEuen, P.L. Thermal transport measurements of individual multiwalled carbon nanotubes. *Physical Review Letters*;8721(21):215502.

21. Zhang, X., Fujiwara, S., Fujii, M. Measurements of thermal conductivity and electrical conductivity of a single carbon fiber. *International Journal of Thermophysics* 1999;21(4):965-980.

22. Fujii, M., Zhang, X., Xie, H.Q., Ago, H., Takahashi, K., Ikuta, T., Abe, H., Shimizu, T. Measuring the thermal conductivity of a single carbon nanotube. *Physical Review Letters* 2005;95(6):065502.

23. Dames, C., Chen, S., Harris, C. T., Huang, J. Y., Ren, Z. F., Dresselhaus, M. S., et al. A hot-wire probe for thermal measurements of nanowires and nanotubes inside a transmission electron microscope. *Review of Scientific Instruments* 2007;78(10):104903.

24. Wang JL, Gu M, Zhang X, Song Y. Thermal conductivity measurement of an individual fibre using a T type probe method. J Phys D 2009;42(10):105502.

25. Cahill DG. Thermal conductivity measurement from 30 to 750 K: the 3ω method. Rev Scientific Instruments 1990;61:802.

26. Choi, T.Y., Poulikakos, D. Measurement of thermal conductivity of individual multiwalled carbon nanotubes by the 3-ω method. *Applied Physics Letters* 2005;87:013108.

27. Zhang, Y., Christofferson, J., Shakouri, A., Li, D. Y., Majumdar, A., Wu, Y. Y., et al. Characterization of heat transfer along a silicon nanowire using thermoreflectance technique. *Ieee Transactions on Nanotechnology* 2006; *5*(1): 67-74.

28. Hou, J. B., Wang, X. W., & Guo, J. Q. (2006). Thermal characterization of micro/nanoscale conductive and non-conductive wires based on optical heating and electrical thermal sensing. *Journal of Physics D-Applied Physics, 39*(15), 3362-3370.

29. Wang, T., Wang, X., Guo, J., Luo, Z., & Cen, K. (2007). Characterization of thermal diffusivity of micro/nanoscale wires by transient photo-electro-thermal technique. *Applied Physics A-Materials Science & Processing, 87*(4), 599-605.

30. Guo, J., Wang, X. Thermal characterization of microscale conductive and nonconductive wires using transient electrothermal technique. *Journal of Applied Physics* 2007;101:063537.

31. Guo, J. Q., Wang, X. W., Zhang, L. J., & Wang, T. (2007). Transient thermal characterization of micro/submicroscale polyacrylonitrile wires. *Applied Physics A-Materials Science & Processing, 89*(1), 153-156.

32. Demko, M.T., Dai, Z.T., Yan, H., King, W.P., Cakmak, M., Abramson, A.R. Application of the thermal flash technique for low thermal diffusivity micro/nanofibers. *Review of Scientific Instruments* 2009;80(3): 036103.

33. W. Voigt, Uber die Bezichungen zwischen den beiden Elastizitaskonstanen isotroper Korper. *Wied Ann* 1889;**38:**573–587.

34. Kim, H.S. On the rule of mixtures for the hardness of particle reinforced composites. *Materials Science and Engineering* 2000;289(1):30-33

35. Chen YM, Ting JM. Ultra high thermal conductivity composites. *Carbon* 2002;40(3):359-362.

36. Singh U, Prakash V, Abramson A. Mechanical characterization device for in situ measurement of nanomechanical properties of micro/nanostructures. *Applied Physics Letters* 2006;89:073103

37. Carslaw, H., S., & Jaeger, J.C. (1959). *Conduction of Heat in Solids*, 303.